The Effect of Mass Irregularities on the Response of Inter-Storey Drift and Floor Accelerations for Isolated and Un-Isolated Structures

A thesis
submitted in partial fulfilment
of the requirements for the Degree
of
Masters in Engineering
in the
University of Canterbury

by

Waller, Alastair James

UNIVERSITY OF CANTERBURY
CHRISTCHURCH, NEW ZEALAND

MAY 2010

Abstract

The use of base isolation to help mitigate and reduce the effects of earthquake excitations has become common place on many important structures. There is also a larger amount of heavier machinery and equipment being stored in some of these important structures; this means that there is a possibility that there are mass irregularities with in a structure. While the response of structures that have been base isolated has been studied they are typically design with floors having a uniform mass. This thesis investigates how mass irregularities affect the response of the floor accelerations and inter-storey drifts within a flexural structure with and without a base isolation unit. The ductility demand of the isolator unit is also investigated at during the course of the analysis. The reason for observing the response of the structure is because often in building design there is a need to have floors that have larger masses then the rest of the structure, and understanding how these mass irregularities affect the response of the structure, then the designing of such structures will be simpler during the initial concept stage.

Acknowledgements

I would like to extend my thanks to the Department of Civil Engineering for the opportunity to do the thesis at the University of Canterbury.

I would also like to thank my supervisors, Dr Athol Carr and Dr Bruce Deam, for without their support, knowledge and assistance I would have never done this Thesis.

And to my parents, John and Joyce Waller, I would like to give my best regards for their support during the research process.

Contents

1 Introduction

In most designs for seismically active regions an elastic design of a structure is not economical and so alternative methods are desired so as to reduce cost. This thesis will briefly look the use of un-isolated plastic design, followed by an investigation of base isolation as a seismic resisting system. The design of most structures for seismic resistance is based on response spectra produced from previous earthquakes. The current New Zealand design spectra Figure 1.1, reproduced from NZS 1170.5 (Standards New Zealand. 2004), shows that for stiff structures the accelerations developed during an earthquake are high, but reduce with an increase in the natural period of free vibration of the structure. This means that for short period structures the cost of building an elastic structure can be uneconomical. This cost is usually mitigated by introduction of a ductile response into the behaviour of the structure through the use of plastic hinges and other hysteretic member behaviour as the result of yielding or by other forms of energy dissipation by the structural elements. This process allows for a reduction in the maximum acceleration response of the structure. However, as a consequence the maximum displacement increases as a result of the increase in the natural period of free vibration.

The ductility that a structure provides during a high excitation event is obtained from the non-linear behaviour of the material and in most cases, due to hysteretic behaviour, re-centring of the member does not occur. This means that even if a structure is still standing after the earthquake it may not be serviceable due to large residual displacements and rotations. With base isolation all the deformation is designed to be constrained within the Isolation unit, thus allowing for the building to remain serviceable as no structural damage occurs in the other elements.

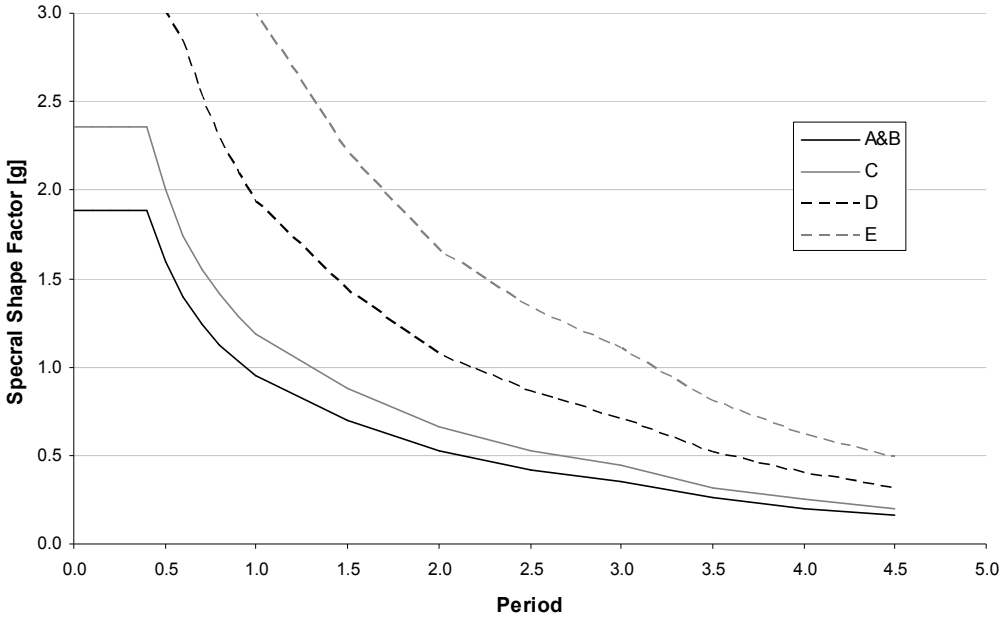

Figure 1.1 Plot of New Zealand Acceleration Design Spectra

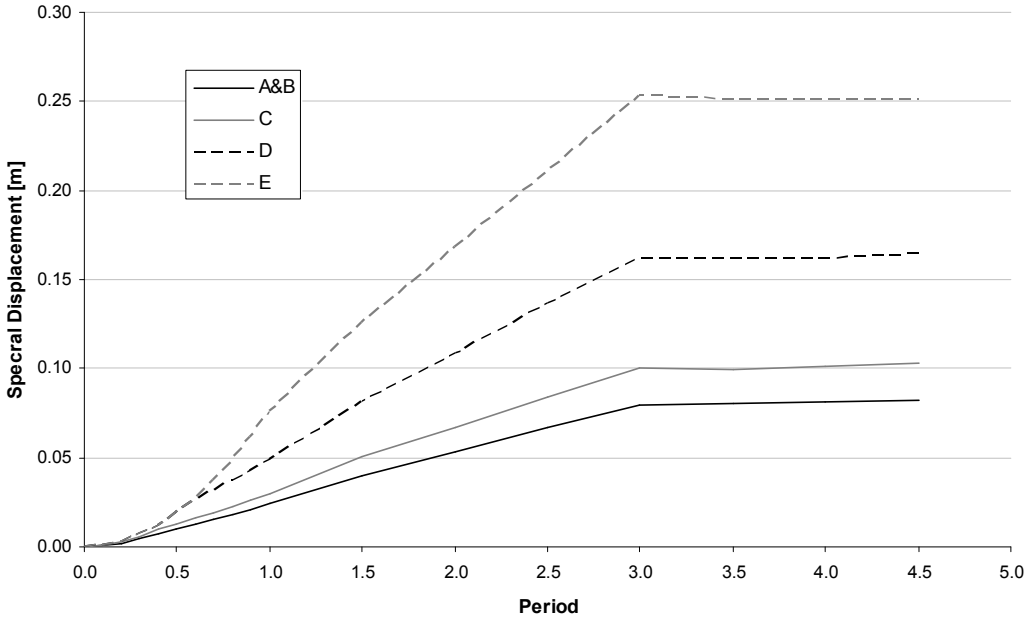

Figure 1.2 Plot of New Zealand Displacement Design Spectra

1.1 Objectives of the Thesis

The objective of the thesis is to observe the effects of mass irregularities on the floor accelerations and inter-storey drifts of a flexural structure. The structure will be subjected to a suite of earthquake records, and a statistical analysis will be conducted to obtain a more realistic response of the structure.

1.2 Scope and Outline of the Thesis

This thesis seeks to present the response of a structure, un-isolated and isolated, subjected to earthquake excitations. The maximum floor accelerations and maximum inter-storey drifts with corresponding cost due to expected damage will be used to make recommendations about the locations of where mass irregularities should be located. The ductility of the isolator will also be considered to observe the effects that the mass irregularities has upon the isolator units.

Chapters 2 through to chapter 5 will give background information on base isolation and earthquake records, along with design procedures for base isolators and how the earthquake records where scaled to give the required spectra for the different return periods. Chapter 6 explains the development of the structure and model, as well as outlining the methods used to obtain the average inter-storey drifts and floor accelerations.

Chapter 7 discusses the results obtained during the research undertaken as part of the thesis, with conclusions, recommendations for practice and future research in the following three chapters.

2 Literature Review

2.1 Previous Studies

The early effects of base isolation on structures where modelled by using a bi-linear hysteretic rule (Andriono, Carr et al. 1990). In most cases this is not a bad approximation as most base isolation units have a well defined yield point. However, as new materials become available, the response of the unit under loading has become more complex. One example of this is the High Damping Rubber unit (Grant, Fenves et al. 2005) where the material shows an almost tri-linear behaviour with increasing stiffness with increased strains, allowing for a constraint on the deformations. A new base isolation unit is currently being tested and investigated (Pocanschi and Phocas 2006) where a glass-fibre reinforced epoxy resin ball is surrounded by a ring of layered rubber and steel plates. The ring acts as the vertical stiffness of the unit; while the ball, which is embedded between two concave elastomeric pillows, takes the shear force and has an increasing stiffness with deformation. As this is a very recent development, this thesis will not investigate its use further, but may relate to the idea by using the High Damping Rubber unit.

Isolation units or damping devices can be categorised by sub-grouping the units or devices into three main groups; Active, Semi-Active, and Passive devices. This grouping is based on how much reliance there is for external control and power. A good example of this is where additional mass is added to top of tall buildings that allows for a degree of tuned mass damping. The relative moment of the mass is controlled by hydraulic rams and a computer, allowing for greater control over the response of the building. This is Active control as the computer is required to be operational during any excitation using the mass as a damper with external power required to operate the rams. If the computer is required just to change the resistance to the movement of the mass without the use of external power source the system is said to be Semi-active system. If the mass is not controlled by a computer or rams then it is a Passive damper. This is the same for base isolation units, but in base isolation most systems tend to be Passive as maintenance and replacement of the devices can be difficult due to their locations in the structure.

One of the first base isolation units was the Lead Rubber Bearing. This unit consists of laminations of alternating layers of steel and rubber of the order of 3mm thick with a core of lead that passes through the laminations. Figure 2.1 is a diagram that shows the typical layout for a unit. The steel provides a confining stress to the rubber when the unit is loaded vertically, while the lead core provides initial lateral stiffness to the unit. This means that there an elastic response for the accommodation of wind loading on the structure. The value of the yield strength is dependent on both the wind loading and the seismic demand of the structure, though in most cases yield strength is minimised as this gives a better response during earthquake excitation.

Other types of Isolation units are Lead Extrusion devices, torsional or flexural steel beams. All of the Isolation units require hysteretic damping to occur so as to absorb energy from the earthquake motion and transmit a reduced motion to the superstructure. Figure 2.2 shows how each unit behaves with a generalised load – deformation hysteretic plot. It should be noted that as material damping is used in these cases there is no re-centring of the device after the event. This differs from semi-active and active Base Isolation devices that allow for re-centring of the unit after the event.

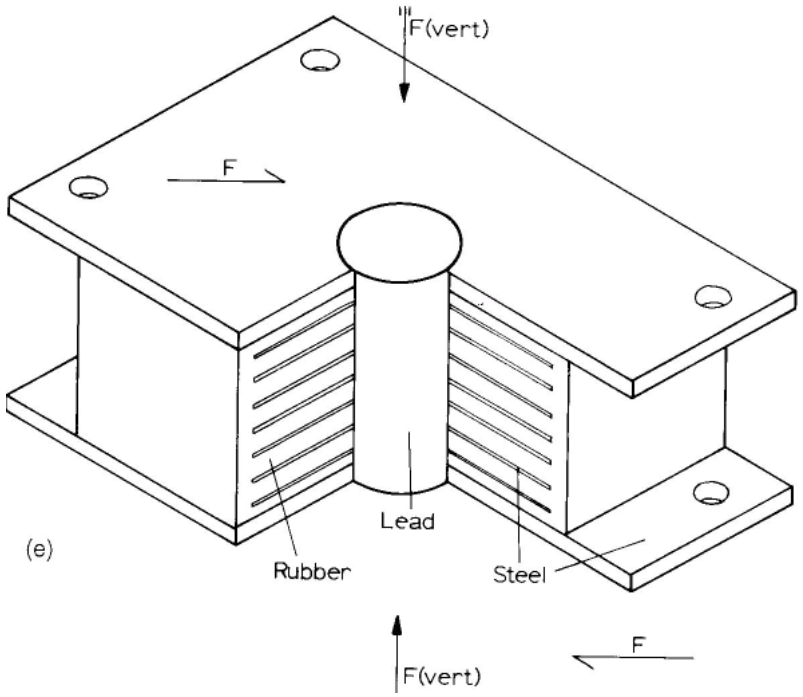

Figure 2.1 Profile of a Laminated Steel-Rubber Bearing unit with a Lead core

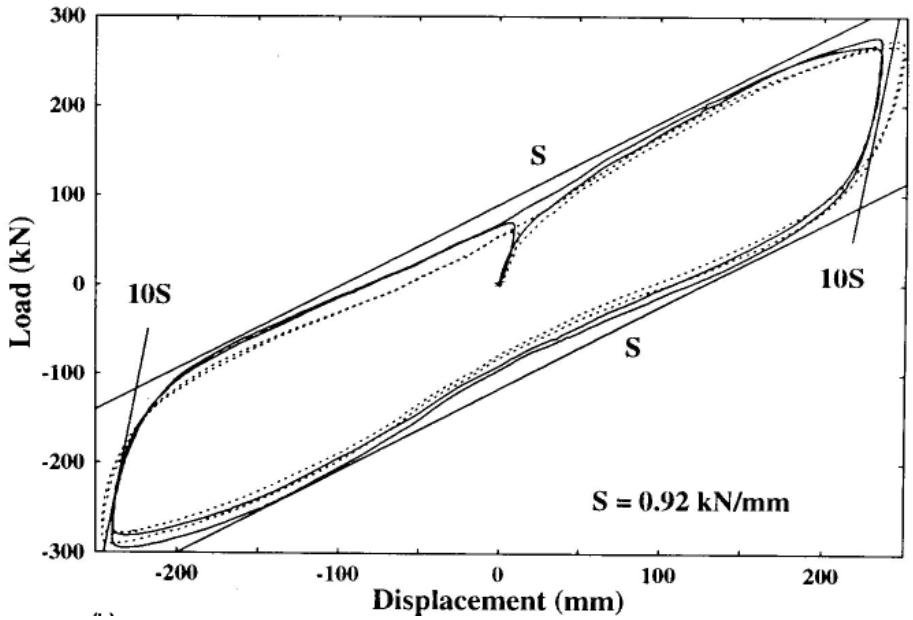

Figure 2.2 The hysteretic loop for a Laminated Steel-Rubber Bearing unit with a Lead core

A common use of base isolation units is to isolate equipment that is sensitive to large accelerations, or is required for post earthquake management, such as medical

equipment. Studies have been conducted for looking at this thru the use of base isolation and the corresponding reliability of the system (Alhan and Gavin 2005) from which it can be shown that there is an optimum design range for Base Isolation. In the paper (Alhan and Gavin 2005) the structure that they analysed had two Isolation systems, the first system was between the foundation and superstructure, the second was between the second floor and a secondary second floor. The study showed that just having the second floor isolation units were effective and if the base was isolated as well, then there was some decrease in the response of the second floor except for the very short frequencies. This is a problem for near-fault isolation as the ground motion has large pulse-like components that can cause large deformations to occur in the base isolation units (Jangid 2006).

Jangid conducted an analytical experiment looking at how to optimise the use of Lead Rubber Bearings in near-fault locations. In this study the parameters that defined the Lead Rubber Bearing were varied to see how the structure would respond to a near-fault earthquake. The parameters that were varied are the yield strength and the yield displacement. The yield displacement had only two values, whereas the yield strength had a range of values. Figure 2.3 shows how the response of the structure varied over the range of yield strength and also shows the response of the Lead Rubber Bearing. For this figure it can also be seen that for low yield force, there is a reduction in the top floor accelerations, however there is a corresponding increase in the lateral displacement of the bearings.

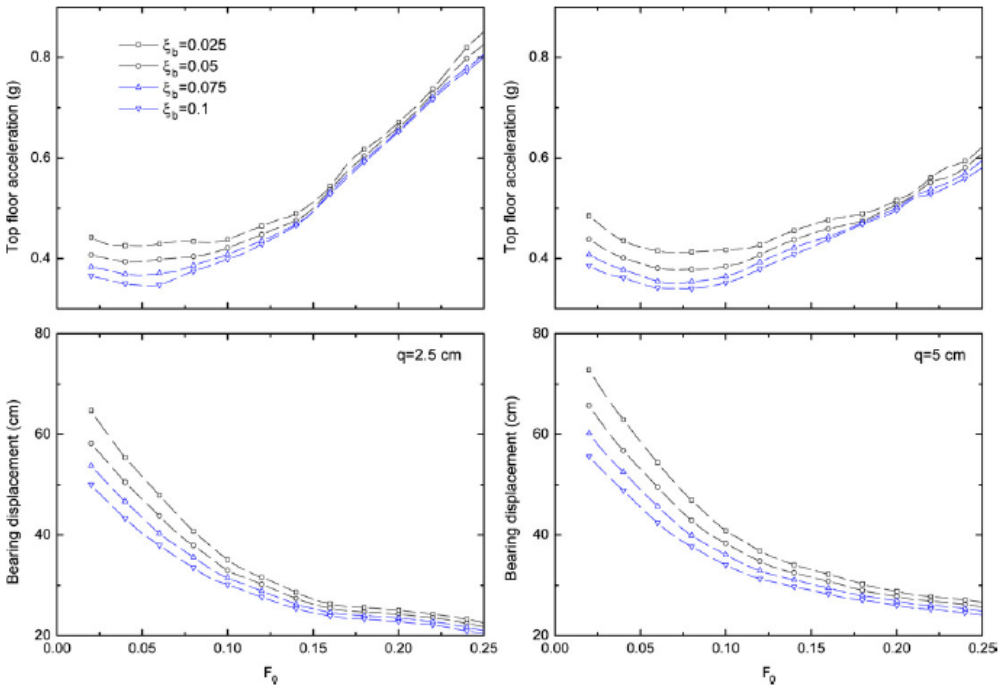

Figure 2.3 Results from Jangid, 2006. Plots show response for different yield displacements (q), and different Lead Rubber Bearings ($F_0=F_y/W$), where W is the weight of the building and F_y is the yield force of the Lead Rubber Bearing

From the study, Jangid was able to express the optimum design force of the Lead Rubber Bearing by Equation 2.1, where Q is the characteristic strength of the lead-core, $M\ddot{x}_a$ is the maximum force exerted in the structure with rigid conditions and k_b is the stiffness of the Lead Rubber Bearing.

$$f(\ddot{x}_a, x_b) = Q + 2k_b x_b + M\ddot{x}_a$$

Equation 2.1 Equation for Optimisation of Lead Rubber Bearing

The minimisation of this equation leads to the optimum design parameters for the Lead Rubber Bearing. However it does not restrict the deformation of the bearing in any way except as part of the combination. This means that the design needs to be checked to ensure that the deformation does not exceed the maximum allowed in the Lead Rubber Bearing.

Other studies of structural performance include the use of resilient-friction base isolation systems (Hong and Kim 2004), isolators with increasing stiffness to prevent

excessive deformation (Pocanschi and Phocas 2006) and how reliably equipment can be protected for earthquake excitations (Alhan and Gavin 2005).

Previous studies by Skinner, Robinson and McVerry have shown that for a base isolated structure that the first mode dominates the deflection of the structure with the possibility of higher modes making a significant contribution to the response of floor accelerations and possibly the inter-storey drifts. They concluded in their report that the main factor of this was the Non-Linearity factor NL, which for a Bi-Linear Isolator is defined as

$$NL = Q_y / S_b - X_y / X_b$$

Equation 2.2 Equation for the determination of the Non-Linear factor according to Skinner

where Q_y and S_b are the yielding and ultimate capacities, and X_y and X_b are the yielding and ultimate displacements. This value NL varies between 0 and 1 and the response of the top floor acceleration tends to increase linearly with the Non-Linear factor.

NCEER Vol 5, #3

3D – Basis is a program developed and verified at the University of Buffalo in conjunction with researchers from the University of Missouri at Columbia. It is a modelling program developed for use to determine the response of a structure during earthquake events, with or without, base Isolation. The program was originally designed for use as an aid to construct test specimens and as a design tool for Sliding Isolators devices; this leads to the joint study of the development of

NCEER Vol 7, #3

NCEER in conjunction with Taisei Corp. of Japan investigated the use of a semi-active Isolation device labelled as the Hybrid Sliding Isolation System. This device is a variable friction device where the friction is changed using a pressurised fluid. This device appeared to perform well under tests that had no restoring forces by using a controller that gave maximum friction when the velocity was in the same direction as the displacement and minimum friction when the velocity was opposite of the displacement, this meant maximum restoring force and minimum offsetting force. By

doing this during the tests, a reasonable reduction in the accelerations transmitted to the structure and the displacements were controlled in order to prevent loss of bearing. Also of note is that this unit is only “sealed” when the vertical force exerted by the superstructure is compressive, hence the pressure of the fluid and the acceleration of the structure needs to be controlled such that vertical tension forces do not develop across the isolation device.

Most simplified methods that are in use today are based on equivalent static approximations where the fundamental period of the base isolated system is used along with code Spectra to obtain an equivalent base shear. Problems occur because the assumption for most equivalent static solutions is that the first mode of free vibration dominates the response. Research has shown that this is not the case with base isolated structures and so additional base shear is added to the top storey to increase the shear through the structure to compensate for this short coming (Priestley, Crosbie et al. 1978).

2.2 *Examples of Design Methods*

Andriono, Carr (1990)

An example of a simplified method of design is outlined below, this is taken from a research report (Andriono, Carr et al. 1990), not a code. Note: that this method is based on a Bi-Linear approximation of the base isolation unit behaviour.

i) Determine the fundamental period of the un-isolated structure

ii) Make a trial selection for the base isolated system

iii) Assume the maximum displacement ratio, μ

iv) Obtain the effective stiffness of the base isolated system

$$k_{eff} = k_0 (\frac{1-\alpha}{\mu} + \alpha)$$

where

k_0 is the initial isolator stiffness

k_{eff} is the effective isolator stiffness

μ is the equivalent structure ductility

α is the isolator ductility

v) Determine additional damping due to hysteretic behaviour of the base isolation unit

$$Add.\lambda = E_h = \frac{2}{\pi} R$$

$$R = (1-\alpha)(\frac{\mu-1}{\mu^2})\frac{k_0}{k_{eff}}$$

where

R is the ratio of hysteretic loop area to the area of its enclosing rectangle

vi) Determine the fundamental period of the base isolated system

vii) Calculate the base shear based on period and damping, calculate maximum displacement of the system

viii) Compare maximum displacement ratio; if there is a difference, refine the assumed maximum displacement ratio and redo steps iv to viii.

ix) Detail base isolation unit

x) Determine the equivalent static forces based on the appropriate loadings code

xi) Design superstructure using elastic design principles. Use capacity design concepts to allow for earthquakes above the design level

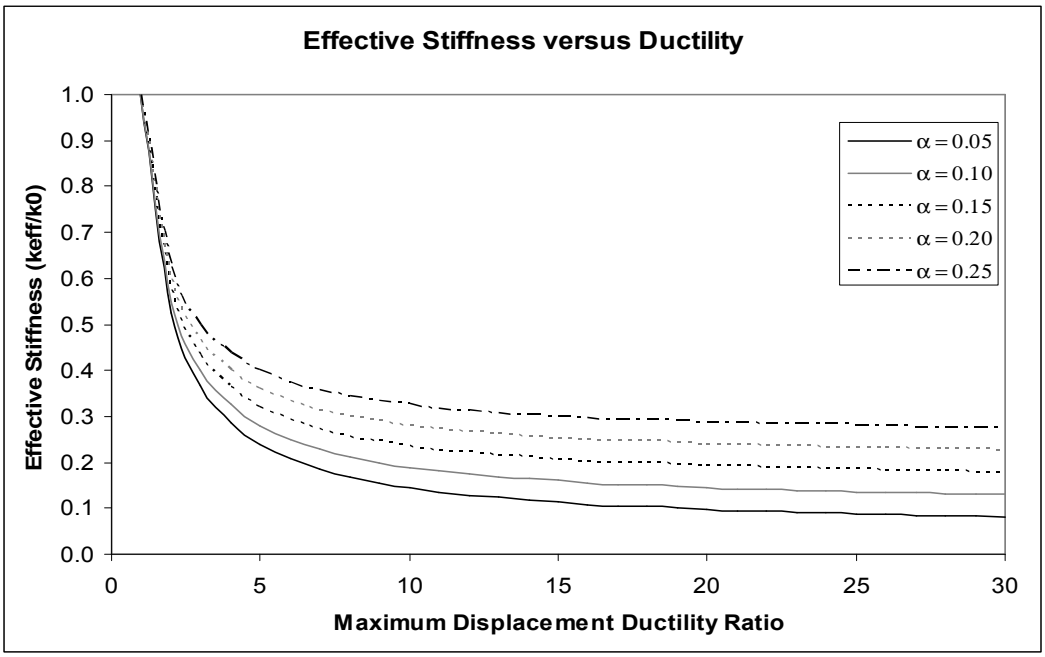

Figure 2.4 Plot of Effective Stiffness due to Base Isolation

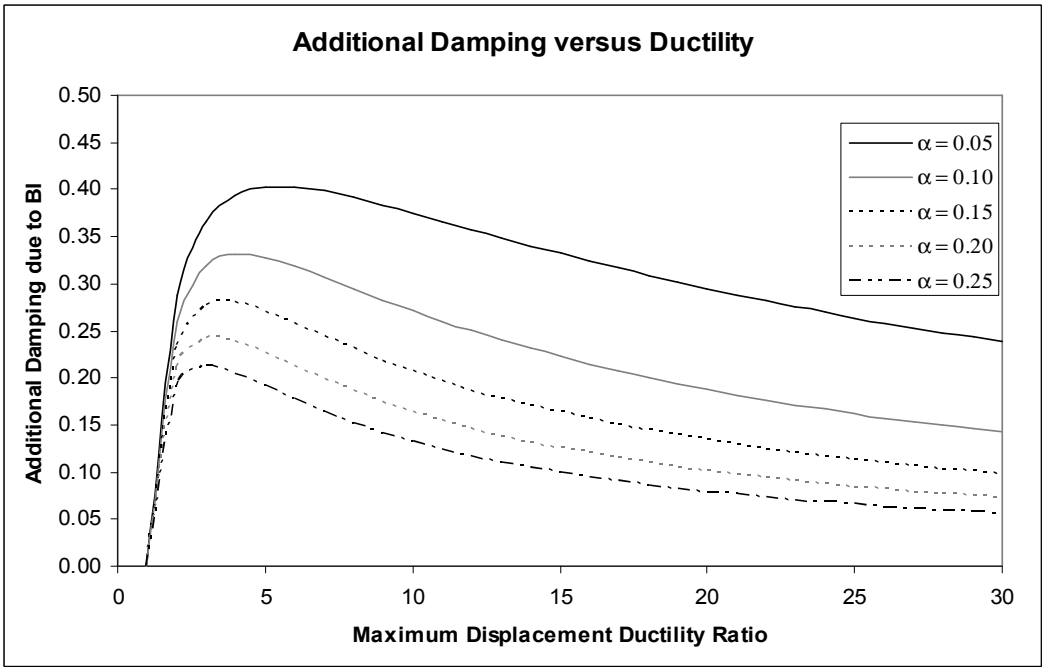

Figure 2.5 Plot of Additional Damping due to Base Isolation

Earthquake Engineering Handbook

High Damping Rubber Bearings, based on IBC 2000 Design Parameter

1. Specify the soil condition for the isolation structure
2. Select the design shear strain γ_{max} and the effective damping ratio ξ_{eff} for the bearing, and the target design period T_D for the isolated structure. The former can be obtained from the material supplier.
3. Use code formulas, or static or dynamic analysis, to determine the effective horizontal stiffness K_{eff} and maximum horizontal (design) displacement D of the bearing
4. Select the material properties. Including Young's modulus E and shear modulus G, from the manufacturer's test report
5. Calculate the total height of rubber, t_r, in the bearing according to the design displacement D and design shear strain γ_{max}:

$$t_r = \frac{D}{\gamma_{\max}}$$

6. Calculate the effective area A and thickness t of individual rubber layers
   a. Select the shape factor S under no rocking conditions:

$$\frac{K_v}{K_h} = \frac{\frac{E_c \cdot A}{t_r}}{\frac{G \cdot A}{t_r}} = \frac{E_c}{G} = \frac{E \cdot (1 + 2kS^2)}{G} \geq 400 \text{ for } S > 10$$

Equation 2.3 Equation to determine the Stiffness Ratio

where

K_v = vertical stiffness of the bearing

K_h = horizontal stiffness of the bearing

G = shear modulus, in the range of 0.4 to 1.0 MPa

E = Young's modulus, in the range of 1.5 to 5.0 MPa

E_c = compression modulus of the rubber-steel composite, $E_c = E(1 + 2kS^2)$

A = full cross-sectional area (loaded area) of the bearing

t_r = total height of rubber layers

k = modified factor, in the range of 1 to 0.5

S = shape factor = A/A_f [Kelly, 1993]

A_f = load-free area around the bearing

In Equation 2.3, the stiffness ration K_v/K_h is required to be greater than 400 for S > 10, since the P-δ effect has been ignored in computing the horizontal stiffness K_h. The material constants G, E, and k can be related to the rubber hardness; if no published data are available, G and E should be determine by test.

b. Determine the effective cross-sectional area A_0 of the bearing based on the allowable stress σ_c for the vertical load case P_{DL+LL}:

$$\sigma_c = \frac{P_{DL+LL}}{A_0} \leq 80\, kgf/cm^2 = 7.84\, MN/m^2$$

c. Determine the effective cross-sectional area A_1 of the bearing from the shear strain due to the vertical load P_{DL+LL}:

$$\gamma_c\big|_{DL+LL} = 6S\frac{P_{PL+LL}}{E_c A_1} \leq \frac{\varepsilon_b}{3}$$

Where ε_b is the elongation of rubber at its breaking point. The limit of $\varepsilon_b/3$ is selected according to the American Association of State Highway and Transportation Officials [1983] Guide Specifications

d. Obtain the minimum cross-section area A_{sf} for shear failure of the bearing:

$$A_{sf} = \frac{K_{eff} \cdot t_r}{G}$$

Use A_{sf} to determine the dimensions of the bearing. Then compute the effective cross-sectional area A_2 as the reduced area A_{re} given below:

$$A_{re} = L \cdot (B - \Delta_S) \text{ for a rectangle bearing}$$

$$A_{re} = \frac{d^2}{4} \cdot (\beta - \sin\beta) \text{ for a circular bearing}$$

$$\beta = 2\cos^{-1}\left(\frac{\Delta_S}{d}\right)$$

where

L,B = plan dimensions of the bearing perpendicular and parallel to the displacement, respectively

Δ_S = horizontal displacement of the bearing

e. The design cross-sectional area A of the bearing is the maximum of the three values computed: A_0, A_1 and A_2

f. Select proper dimensions for the rubber layer based on the design cross-sectional area *A*

7. Single layer thickness, *t*, and number of rubber layers

a. Use the shape factor *S* and dimensions of the rubber layer to determine the thickness of individual rubber layer, *t*:

$$S = \frac{L \cdot B}{2(L+B) \cdot t} \text{ for a rectangular bearing}$$

$$S = \frac{\pi d^2/4}{\pi d t} = \frac{d}{4t} \text{ for a circular bearing}$$

where

L,B = plan dimensions of a rectangle bearing (*L*≤*B*)

d = diameter of a circular bearing

t = thickness of individual rubber layers

b. Use $t_r = N \times t$ to determine the required number of rubber layers, *N*

8. Steel plate thickness, t_s:

$$t_s \geq \frac{2(t_i + t_{i+1}) \cdot P_{DL+LL}}{A_{re} \cdot F_S} \geq 2 \text{ mm}$$

where

t_i, t_{i+1} = rubber layer thickness in top and bottom of the steel plate

F_s = 0.6 F_y

F_y = yield strength of the steel plates (= 274.4 MN/m^2)

A_{re} = reduced cross-sectional area of the bearing area under horizontal displacement

9. All the parameters determined for the bearing should be checked against the shear strain and stability conditions given below. If these requirements cannot be satisfied, then repeat steps 2 to 8 for an improved design.

Parameter Checks

1. The rubber layers selected should satisfy the shear strain requirement under the vertical load P_{DL+LL}:

$$\gamma_{c,DL+LL} = 6S \cdot \varepsilon_c = 6S \cdot \frac{P_{DL+LL}}{E_c \cdot A} \leq \frac{\varepsilon_b}{3}$$

where

$$\varepsilon_c = \frac{\Delta_c}{t_r} = \frac{P_{DL+LL}}{E_c \cdot A}$$

Δ_c = compression displacement of the bearing

ε_b = elongation of rubber at break

2. Stability condition: To prevent the bearing from becoming unstable, the average compressive stress σ_c of the bearing should be less than a preset tolerance:

$$\sigma_c = \frac{P}{A} < \sigma_{cr} = \frac{G \cdot S \cdot L}{2.5 \cdot t_r}$$

where L is the least plan dimension of the rectangle bearing or the diameter d of the circular bearing. It should be noted that the following formulas were used by Naeim and Kelly [1999].

$$\sigma_{cr} = \frac{\pi G \cdot S \cdot L}{\sqrt{6} \cdot t_r} \text{ for a rectangular bearing}$$

$$\sigma_{cr} = \frac{\pi G \cdot S \cdot d}{2\sqrt{2} \cdot t_r} \text{ for a circular bearing}$$

3. Shear strain condition for the earthquake load:

$$\gamma_{sc} + \gamma_{eq} + \gamma_{sr} \leq 0.75\varepsilon_b$$

with

$$\gamma_{sc} = 6S \cdot \frac{P_{DL+LL+DL}}{E_c \cdot A_{re}}$$

$$\gamma_{eq} = \frac{D}{t_r}$$

$$\gamma_{sr} = \frac{B^2 \cdot \theta}{2 \cdot t \cdot t_r}$$

$$\theta = \frac{B^2 De}{b^2 + d^2}$$

where

γ_{sc} = shear strain under compression

$P_{DL+LL+EQ}$ = combination of dead load, live load and earthquake load

γ_{eq} = shear strain under earthquake

γ_{sr} = shear strain under rotation

θ = rotation angle of the bearing induced by earthquake

e = actual eccentricity + 5% of accidental eccentricity

b,d = dimensions of the structure with rectangular plan

4. To avoid rollout of the bearing, the displacement of the bearing under the earthquake load should satisfy the following condition:

$$D \le \delta_{roll-out} = \frac{P_{DL+LL+EQ}}{P_{DL+LL+EQ} + K_{eff} \cdot h}$$

where

K_{eff} = effective stiffness of the bearing

h = total height of the bearing (rubber plus steel)

L = least plan dimension of a rectangular bearing or diameter d of a circular bearing

European Seismic Design Practice

(Elnashai and Society of Earthquake and Civil Engineering Dynamics. 1995)

This is done by treating the base isolation unit as a short Beam-Column element with low shear stiffness. This leads to relationship between shear stiffness and vertical loading.

P = Vertical Load
a = radius of steel plates
G = Shear modulus
K = Bulk modulus
h = thickness of rubber layers
t = thickness of steel shim

Compressive stiffness of the bearing

$$k_c \cong \frac{1}{n}\frac{A}{h}\left(\frac{1}{6GS^2}+\frac{4}{3K}\right)^{-1}$$ **Equation 2.4**

$S=\frac{a}{2h}$ Shape factor for bearing unit

$A=\pi a^2$ Area of effective bearing area **Equation 2.5**

Stress in the middle of the steel plate due to vertical loading

$$\sigma=(1.65h/t)P/A$$ **Equation 2.6**

In order to analyse the base isolation unit, this procedure converts the unit into a short Beam-Column and using the following parameters to enable the use in Beam-Column theory.

L = active “length” of unit
R = shear stiffness of unit
B = Bending stiff of unit
H = h + t

$$R = HGA/h$$

$$B = H\left(Aa^2/4h\right)\left(\frac{1}{2GS^2}+\frac{3}{2K}\right)^{-1}$$

$$L = nH$$

Effective shear stiffness of the base isolation unit

$$k_s = \frac{P^2}{2qB\tan(qL/2) - PL}$$

where $q^2 = \frac{P}{B}\left(\frac{P}{R}+1\right)$

Critical buckling load

$$P_{cr} = \frac{R}{2}\left(\sqrt{1+4\pi^2 B/RL^2}-1\right)$$

$$\cong \frac{\pi}{L}\sqrt{RB}$$

Typically, P ≤ 1/3 P_{cr}, thus

$$k_s \cong \frac{GA}{nh}$$

Bearing Roll out check

$$d_{roll} = \frac{2aP}{k_s\left(L+2\Delta L\right)+P}$$

3 Base Isolation

Base isolation is the process of adding flexible, ductile elements to the design of a structure, usually in between the foundation and superstructure. The reason for this process is to increase the fundamental period of the structure. The theory behind this is that for longer period structures the accelerations induced by earthquake motions are reduced. This is similar to the use of member ductility and post-yield behaviour as both methods aim to reduce forces through energy dissipation. The difference here is that for the use of plastic hinges to provide ductility results in the formation of member damage in the local area of the hinge and the possibility of the building being unable to perform normal services. The use of base isolation is to contain the energy dissipation to the units and all damage is located here, which is typically designed to be minimal. A major problem of many forms of base isolation is that there is often a residual displacement due to the hysteretic behaviour of the units, hence the effects of P-δ can be increased and a gradual gravity failure post excitation could result. This is usually taken into account through the determination of Maximum likely displacement that is expected from an earthquake.

3.1 The Physics behind Seismic Isolation

Base isolation increases the period of free vibration of the structure by making it more flexible; thus the large amplitude, short period pulses of the earthquake do not excite the structure as strongly as it would on a shorter period structure. The problem with this is that for near-fault earthquakes there is a significant large amplitude pulse with a longer period, thus the Isolation unit can often underground significant lateral deformation. While in most cases this is not a problem, there is potential for problems due to large deformation. These problems include rolling out, where the bearing deforms to such an extent that P-delta effects cause the building to roll off of the Isolation units, the Isolation units runs out of “travel”, this is mostly likely to affect Isolation systems that have rams or other such connections. An example of this is the Ring-Spring damping device; this has to be pre-stressed in order for tension to be carried across the element. If the tension force exceeds the pre-stressing force, then there is a sudden loss of strength as the unit has run out of “travel”.

Seismic Isolation of structures obtains its effectiveness by increasing the flexibility of a structure; this can be problematic as there is usually in corresponding increase in the displacement response of the structure. This side effect is usually controlled by introducing damping into the structure; this damping can be provided in the form of material hysteretic damping provided by yielding of an element within the Isolation unit or can be provided through friction such as with a piston being driven through a viscous material. For a Lead Rubber Bearing the material hysteretic damping is provided by yielding of the lead core within the unit, while for dash-pot or vicious dampers the relative velocity of piston to the drum provides the friction.

From (Skinner, Robinson et al. 1993) the definition for the Non-Linearity of a bi-linear Isolator will be adopted, but using slightly different notation. The equation for this factor is

$$NL = Q_y / S_b - X_y / X_b$$

where Q_y and X_y are the yield strength and displacement respectively and S_b and X_b are respectively the maximum force applied and displacement achieved. It should be noted that this equation is based on an assumption that the Isolator displaces an equal distance in both directions. For the purposes of this thesis the above equation shall be reformed into the expression

$$NL = \frac{(\mu - 1)(1 - r)}{\mu(1 + r(\mu - 1))}$$

for which it can be seen that the Non-Linearity factor is based on 2 parameters; r, which is the ratio between post-yield and pre-yield stiffness, and μ, which is the maximum ductility achieved during an earthquake excitation. The post-yield to pre-yield stiffness factor r can be easily calculated before design by using the ratio of the pre- and post- yielding tangential periods, hence

$$r = \left(\frac{T_1}{T_2} \right)^2$$

where T_1 and T_2 are the pre- and post-yield natural periods of free vibrations, respectively. The ductility of the isolator is usually determined before-hand, but for a given excitation there is not necessarily a symmetric response from the isolator.

However, for design purposes it is assumed that the response is symmetric as the "direction" of excitation is unknown and the isolation unit reaches its design displacement during the excitation event.

In this thesis the value of both the directions will calculated and an average value will be given. It should be noted that in this case there may be some error as the hysteretic loop may not fully develop due to asymmetric response of the isolator. Also, the parameter r varies between 0 and 1, while μ is always larger then 1. This means that as r approaches 1 the value of NL approaches 0; and the lower the value of μ the lower the value of NL. These two factors mean that for a NL close to zero indicating a low rate dissipation of energy, while a value close to 1 means that there is a large amount of energy dissipation. For a large value of initial isolated period, T_1, over un-isolated period, T_{1u}, Skinner et al. showed that higher modes accelerations do dominate the response of the higher floors, for most cases this is not a problem, for this thesis the un-isolated structure has a period of approximately 1.4 to 1.6s, so for the structures investigated in this thesis values for the initial isolated period will vary between approximately between 1.5 and 2.0s.

		r		
		0.05	0.10	0.20
μ	5	0.633	0.514	0.356
	10	0.590	0.426	0.257
	20	0.463	0.295	0.158

Table 3.1 Table of NL factors for the given r and μ values

Figure 3.1 and Figure 3.2 are plots show how the NL factor changes for different values of r and μ. Figure 3.1 shows how the variation in NL changes for different stiffness ratio values while the ductility is held constant, whereas Figure 3.2 has a constant stiffness ratio, but with varying ductility. The figures show that the effectiveness of a base isolator is changing depending on the demand on the unit in question. For lower levels of ductility demand there is good efficiency with moderate and low stiffness ratios, however, when the ductility demand is increased there is a significant decrease in the effectiveness of the base isolator even with low stiffness ratios. This is because increasing the ductility demand "stretches" the area enclosed

of the outer box, and thus the Isolator hysteresis loop is also “stretched”. The difference between the two is that while the isolator loop only increases in length and not depth, the outer box increases in both depth and length, thus there is always a larger increase in the total potential energy to dissipate then the increase of energy actually dissipated. Initially when the Isolator first starts to yield the efficiency first quickly increases to maximum and then starts to decrease as the ductility demand increases. The effect of the stiffness ratio is more easily seen, for low values, when the ratio approaches zero, the shape of the hysteresis loop approaches that of a rectangle with similar dimensions to the minimum – maximum area, thus energy dissipation is at maximum and as the stiffness ratio increases the Isolator starts to become closer to perfectly elastic and hence there is little to no energy dissipation.

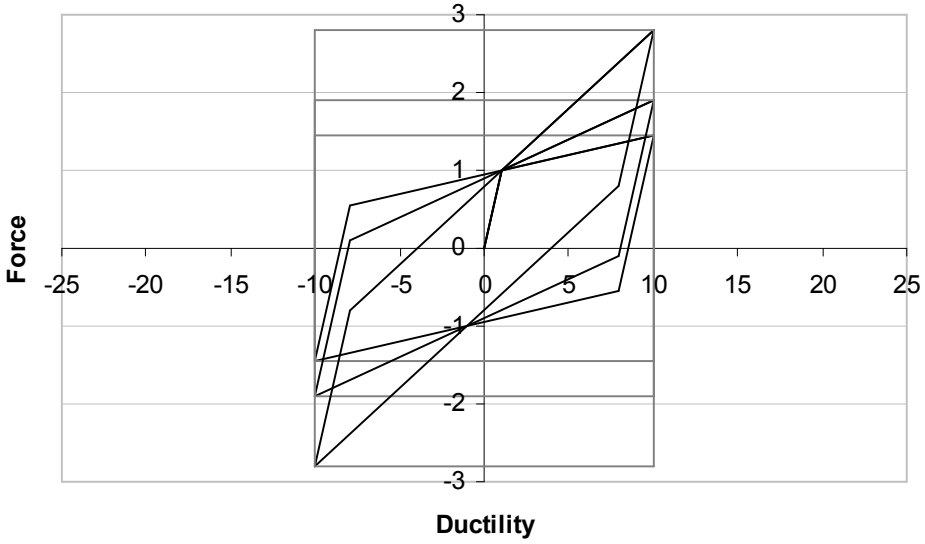

Figure 3.1 Plot showing the effects of Base Isolator variables, in this example the Ductility is held constant at 10 with differing Stiffness Ratio values of 0.05, 0.10 and 0.20.

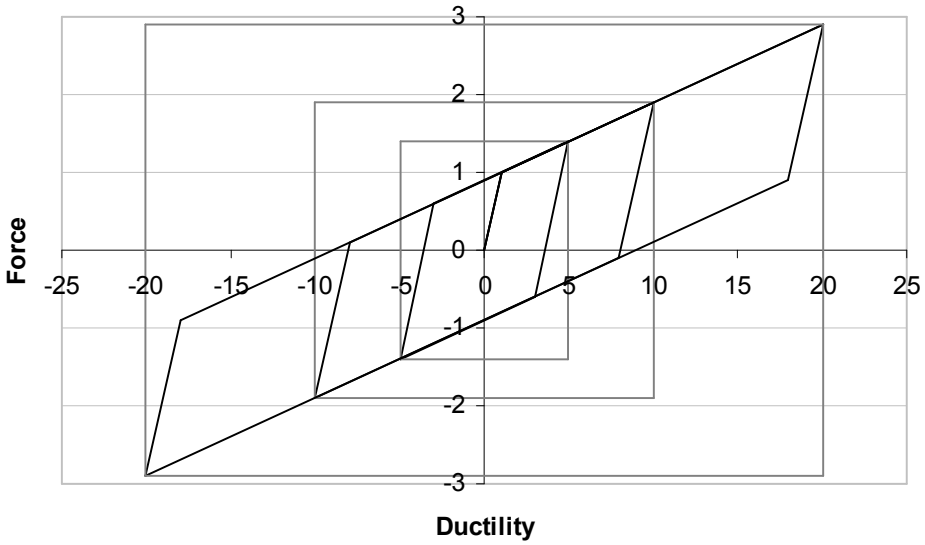

Figure 3.2 Plot showing the effects of Base Isolator variables, in this example the Stiffness Ratio is held constant at 0.10 with differing Ductility values of 5, 10 and 20.

4 Measurements of Earthquake Records

Earthquakes are natural occurring phenomenons that have been identified for many centuries, however, recording of Magnitude and ground movement has been relatively recent in occurrence. The first scale used to record earthquakes was the Mercalli Intensity Scale, followed by the Modified Mercalli Scale; this scale is based on damage caused to mainly masonry structures. However, visual damage is not accurate as different structures perform differently in different earthquakes; also the extent of damage is arbitrary and the assessment can vary widely between two different people. Hence there was a need to develop a more accurate and unbiased earthquake scale, and so the original Richter Magnitude was developed.

Earthquake records are recorded using a device called a seismograph which produces the record as a seismogram. The original seismograms were recorded on paper drums using a pen or stylus, thus gave a continuous analogue record; modern seismograms records are created using digital technology and thus the record is discrete with a constant time interval. The analogue records need to be read by a person in order for any type of simulation to be conducted, there are various methods for this procedure; the minimum and maximum points and their corresponding times are recorded and secondly for the data to be read at constant intervals, similar to that of digitally recorded data. Both methods have positive and negative attributes; the main of which is that taking minimum and maximum give the highest amplitudes, but may miss out important data in between peaks. A second disadvantage is that the time steps are not constant and thus can cause complications for any analyses.

4.1 Earthquake Magnitude

The earthquake magnitude is determined using one of a series of formulae, dependent on the location, depth and other local geology. The formulae use the release of strain energy to calculate the Magnitude, hence the result is less subjective and bias then if an Intensity scales were used. The following is a summary of the different scaling methods and their corresponding limitations, as well as their

corresponding formulae. The following descriptions of the Earthquake Magnitudes are based on the descriptions from McCarthy (McCarthy 2002).

Richter Local Magnitude

Developed in 1935 by Charles Richter this magnitude measurement based on measurements from a Wood-Anderson seismometer. The magnitude was defined by Richter as the base 10 logarithm of the maximum trace amplitude (in micrometers) recorded on a Wood-Anderson seismometer located 100 km from the epicentre of the earthquake. This gives a measure of *local magnitude* which is only applicable to earthquakes with epicentre distances less than 600 km. This Magnitude scale is used for minor to normal earthquakes up to a Magnitude of approximately 5.9, after this the formulae no longer generates the appropriate scaling factor.

Surface Wave Magnitude

Surface waves are the more damaging of the earthquake motions and also propagate further from the source then body waves. Surface waves can be split into two components, Love and Rayleigh waves; Love waves are shear waves that travel outward across the surface and have only a 2D motion, which is radial to the epicentre. Rayleigh waves are rolling waves on the surface on the soil. Both of the surface waves travel slower then body waves, with the Rayleigh waves travelling slower than Love waves; however they tend to be more destructive then the other types of motion. The shear waves are most commonly used for distant earthquakes as both the *P* and *S* waves tend to quickly dissipate. This Magnitude scale is used for earthquakes that exceed the Local Richter Scale but only up to earthquakes of a Magnitude of 8 at which point the Seismic Moment Magnitude scale is used.

Body Wave Magnitude

Body waves are waves that travel through the soil, they travel fast and there are two types of Body waves; the first is a Pulse type of wave that sends compression and dilation zones outwards from the focus, the second type of waves are shear waves that have a planar motion perpendicular to the direction of propagation. The Pulse

waves travel faster than the Shear waves, and hence the Pulse waves and Shear waves are sometimes known as *Primary* and *Secondary* waves. Due to the nature of the Pulse wave, this type of Body wave is able to be transmitted thru both solid and liquid matter, the Shear wave can only be transmitted through solid matter. This method is used for earthquakes with deep focal points.

Seismic Moment Magnitude

Moment Magnitude is measure of the energy released during the event. It is equal to the Area of fault movement multiplied by the average fault movement and also by the Shear Modulus of the soil. This can be a more accurate than other methods as it is independent on type of instruments, and more dependent on the local geography and soil structure. However the measurements of such items as the area of fault activated and average fault slip may be subjective and different through the use of different recording instruments. Also, the shear modulus varies within the soil strata and hence is a further source of inaccuracies. This method is used mainly for large earthquakes as the energy release causes the other methods of become “saturated”, this is when the energy becomes sufficient that the behaviour of the soil has a reduced response to extra energy input from the source.

5 Earthquake Excitations

The use of existing earthquake records to determine the response of structures is the best method as creating an artificial earthquake record can be difficult and not always indicative of the behaviour that a particular fault produces. As such, this thesis will use existing earthquakes records and scale them accordingly for use in the analysis to produce the correct curves for the return periods stated.

5.1 Unscaled Earthquakes Records

These earthquake records have not had their amplitude changed to match any particular Code Design Spectra; they are presented to allow a comparison of the GNS records to that of recorded earthquakes. It should be noted that the Tabas and San Fernando records both exhibit near fault effects and thus is unlikely that the actions of these would occur in a region not associated with any fault activity.

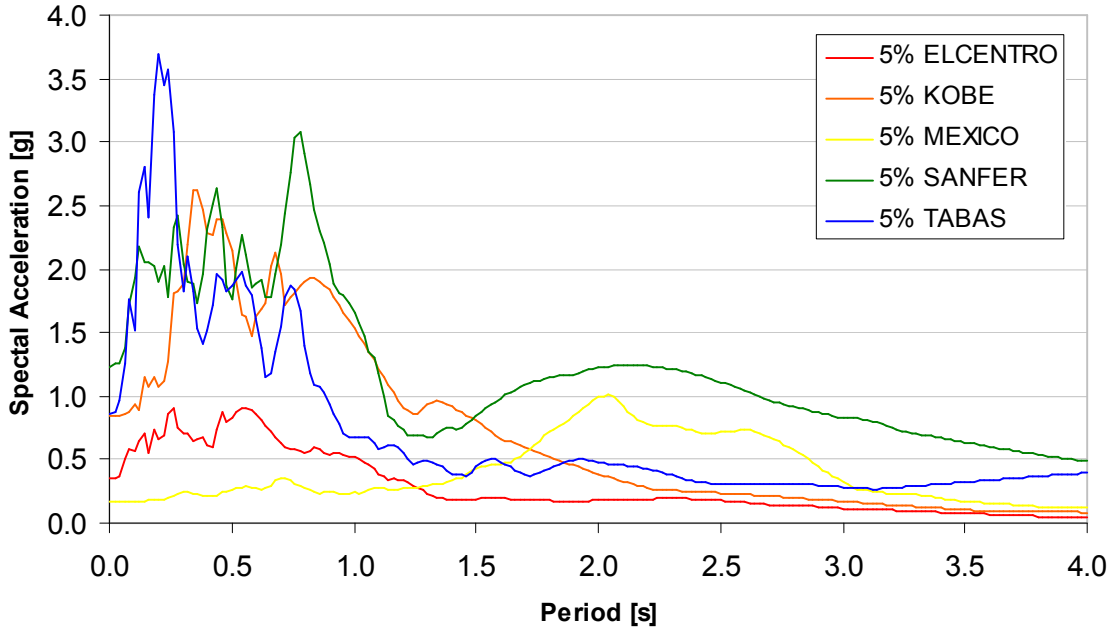

Figure 5.1 Plot of earthquake Spectral Accelerations

The El Centro 1940 earthquake record was chosen to be part of the initial analysis as it is regarded as a typical large excitation earthquake. This was used as a basis for many early analyses until larger earthquakes occurred, however due to the extensive use to which this record was used as a benchmark it still has significant usage in many analyses to date.

The Kobe and San Fernando earthquakes were included as it shows accelerations of near fault earthquakes, which is predominantly large amplitude, but short duration, pulses which can adversely affect the response of the base isolation units. The Tabas record was included as it is one of the largest earthquake records that has occurred in recent history.

The Mexico City earthquake was highly damaging to due the unique nature of the underlying soil strata at the location meant that the long period waves were extravagated and resulted in severe damage to some structures, while other structures merely subsided into the soil with very little structural damage.

5.2 GNS Scaled Records

These records were used as they give a range of different earthquake excitation. Figure 5.3.2 shows the minimum, maximum and quarterly percentiles; these give an indication of the range of excitation provided by the records. Most of the variation occurs with the first 1 second of the natural period range, where most structures are typically located; there is still a reasonable amount of variation through the 1 second to 2 second range, with the variation above 2 seconds being fairly constant.

5.3 Scaled Records used in the Thesis

The earthquake records are to be scaled using the NZS 1170.5 standard. This means that for each return period the spectral acceleration versus period curve needs to be produced and each record to be adjusted so that there is minimum difference between them, using a method such as Least Squares Regression. This means that the average of the earthquake records should approximate the

corresponding Curve from NZS 1170.5 for the range that it is required, which is between 0.4T and 1.3T, where T is the fundamental period of the structure.

Figure 5.2 is a plot of the spectral acceleration curves for the 7 different return periods and Figure 5.3 show the average of the earthquake records and also the 25th and 75th percentiles, as well as the minimum and maximum envelope of all records. The average line is to show what the expected results will be; the percentiles are showing the level of variation that the earthquake records exhibit and the minimum and maximum lines are showing what the maximum spectral acceleration could be.

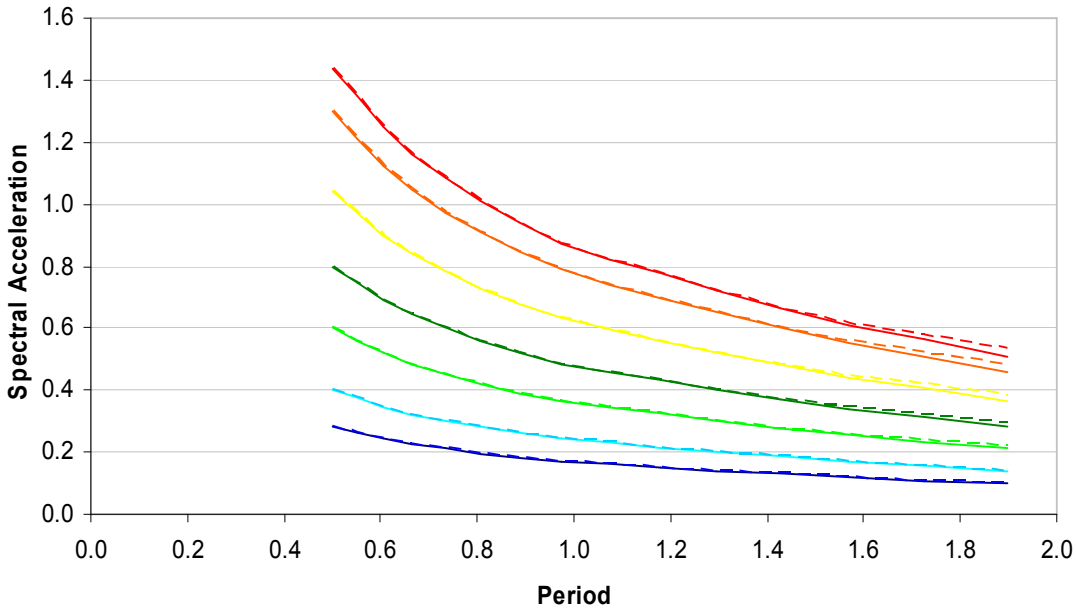

Figure 5.2 Plot showing NZS 1170.5 Design Curves for the different Return Periods

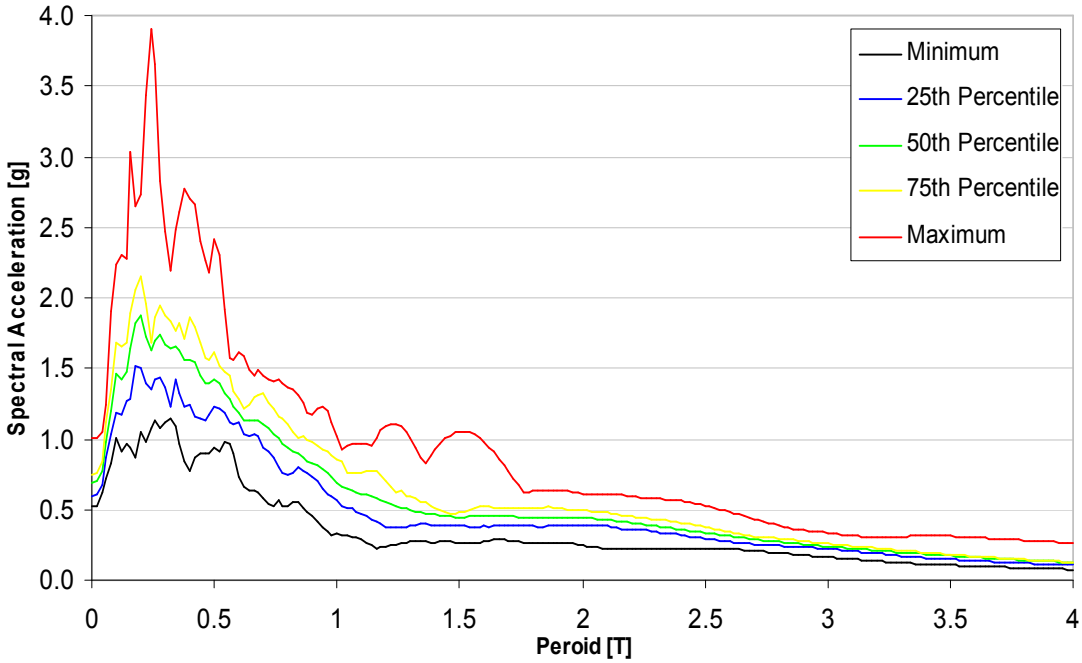

Figure 5.3 Plot showing the Maximum, Minimum and quarterly Percentiles.

6 Methodology

The method for determining the accelerations and forces on the structure is to use a non-linear time history program, in the case of this thesis, Ruaumoko (Carr 2005) was used to conduct all non-linear Structural Analyses. The structure used is a structure designed as a Concrete Steel-Reinforced structure; that has a gravity resisting frame and a shear wall for lateral resistance. The maximum and minimum floor accelerations and inter-storey drifts for each earthquake and structural model will be recorded so that statistical analysis can be conducted on the output. Currently, the thesis shall have 24 different excitation inputs, each with 7 different amplitude scales for the 7 return periods, and for the base isolated structure with mass shifts there will be 144 different structural models that vary in percentage mass shift, location of the mass shift, base isolator yield strength, initial period and post-yield period. The mass shift is based on assuming that, for some unknown reason, part of the structures total mass, in the case of this Thesis it is taken to be 5% and 10%, is shifted to a different location. As the 5% and 10% mass shift is being added the current mass of different floors, each shift gives a different structural response when the structure undergoes earthquake excitation.

6.1 Structural Model

The structural model that was chosen for this thesis is a reinforced concrete structure of eight storeys. This is because concrete is a relatively commonly used material in New Zealand, and an eight storey structure is not overly stiff, nor is it so tall that wind effects govern the lateral design on the structure. Initially the shear wall was designed to carry all of the lateral forces, with the beams and columns carrying only gravity loads. The earthquake coefficient that was used was taken from NZS 1170.5 (Standards New Zealand. 2004) using the criteria of a level 3 structure located in Christchurch, Canterbury. This led to an initial value for the coefficient which was later refined using the stiffness of the shear wall after initial design to ensure that the shear wall had sufficient moment capacity. A simple elevation is shown in Appendix C: Elevation of Building.

The floors use a standard precast double T flooring system, with the beams being either precast off-site and cast-in-place or in-situ. For this thesis the means of construction were not part of the design or analysis. All the columns are the same, and for this analysis were only designed for gravity and hence, axial forces only. Although initial analysis shows that the columns provide some moment resistance, this is due to a force couple between the outside two columns.

The wall was designed through an iterative process to ensure that the moment capacity was not exceeded and the earthquake coefficient is updated using the updated initial stiffness. The initial stiffness determined by calculating the moment and curvature at first yield, the ultimate moment and curvature was also calculated to determine the post yield properties required by Ruaumoko. Note that this is a simplified result as the actual moment-curvature curve is not two straight lines, however for this analysis it should be sufficient. The lowest floor actually has two floors between which the base isolator units are located. This means that the floor mass needs to be taken into account during the computer simulations. It is also taken that the base floor provides enough rigidity to help prevent rocking and hence shall not be considered further in this study, the reason being that base isolation should be designed to prevent the rocking of a structure.

6.2 Computer Model

As with all computational models, a full and complete model is both labour extensive and is not fully accurate, as for concrete the true stress-strain model is not yet fully understood and so the effort put into detail models does not always yield results that justify the effort. Ruaumoko has several different means of forming members and structures, for this thesis the structure was formed using elements that are represented by lines and nodes. For the beam-column joints, the use of rigid ends were used, this is a inbuilt addition in Ruaumoko that allows for the user to adjust where the actual calculations are conducted, so that the effects of overlapping members can be removed. The base isolator unit is represented by a spring element and can only transmit horizontal forces to the structure. The structure is assumed to have a fixed base when it is not base isolated and with base isolation that there is sufficient restraint to prevent any rocking motion. The columns have the same steel

reinforcement but have been checked for 3 different axial compression forces from the gravity weight of the floors and beams. This resulted in 3 different moment capacities due to moment-axial force interaction; therefore the maximum moment capacity is at the bottom of the structure, and the minimum capacity at the top of the structure. It should be noted that because the wall only has its self weight for maximum moment capacity. The moment-axial force interaction diagrams for the columns and wall can be found in Appendix D: Moment-Axial Force Interaction Diagrams of this Thesis, and it can be seen that for the wall, with a self weight of 235kN, that there is a very minor variation of moment for that small axial force, hence is the reason that it is not taken into account for the analysis.

The earthquake excitations were input and the program was run as a batch set of analyses with the minimum and maximum accelerations and drifts recorded from each analysis. The results are recorded in separate files, with an ID recording structural model type, and the earthquakes are run in ascending order with each result following on from the previous. A specific FORTRAN program was produced to calculate the Probability of Exceedence for different return periods, inter – storey drifts and accelerations by calculating the mean and standard deviation using the maximum and minimum points obtained during the analyses. The resulting mean and standard deviations were used to calculate the Probability of Exceedence for the various limit states; for example, drift limit states are based on the expected damage occurring to the structure, and so by calculating the Probability of Exceedence, an estimate of the overall expected damage can be obtained.

6.3 Analysis

Due to there being several different earthquake records at different return periods allows for some statistical analysis to be conducted. Due to the records having been scaled to different intensities fragility curves can be produced, as well as cost estimates if needed. The data will be divided into two main categories, floor accelerations and inter-storey drifts. The results can be split further into groups determined by base isolation stiffness and yield strength, percentage mass shift and location. This is because the maximum acceleration achievable is dependent on the

maximum transferrable shear through the base isolation unit, and by using the percentage Mass change it allows for a second clear division type. Other divisions such as mass location can be expressed more as secondary divisions, as there is little variation between shifting the mass to adjacent levels in the structure, however this effect may not be small for a mass shift from the bottom floor to the roof.

During this part the results for an un-isolated structure will be used as a control set of data, with base isolation and mass shifts being the variables. For most cases the data will be split as to have the different base isolator configurations on the same plot as to minimize the number of data lines. As there are more possible combinations for the location and size of the mass shift, as well as what floor is being considered, so base isolation parameters make more sense as a first filter. The statistical data is assumed to follow a normal distribution and hence, all analysis is carried out using this assumption.

For the analysis of the drift the values in
Table 6.1 were used to calculate the expected damage cost associated with the drift levels achieved during earthquake excitation, it should be noted that the drift of the higher levels will be greater due to the rotation for the lower storeys causing greater deflections at the top of the structure. A significant factor of this is that there may be limited structural damage done to the structure, yet fixings and other non-structural elements may be severely damaged.

Drift Min [%]	Drift Max [%]	DI [%]
-	0.2	0.3
0.2	0.4	3.5
0.4	0.8	10
0.8	1.5	65
1.5	2.5	80
2.5	-	95

Table 6.1 Table with values for Drift Calculations adapted from (Foltz 2004)

Note that in

Table 6.1 there is still damage occurring for the small 0.2% drift, this is due to the minor damage associated with earthquake movement and tends to only affect the non-structural components such as furnishing and equipment, for 0.2% to 0.4% light damage is occurring to the structure as there well be some minor damage to the structural elements will start to occur. 0.4% to 0.8% drift indicates moderate damage to structural elements and also severe damage to the non-structural elements. The drift limit of 1.5% is for life safety of the occupants of the structure, with 2.5% where structural collapse is highly probable.

7 Results

The results from the Ruaumoko Non-Linear Time History analysis were sifted for the minimum and maximum values using a purpose built FORTRAN program; it should be noted that the use of the terms minimum and maximum are to describe the structural response of in the negative and positive direction respectively. The data that was sourced from the Output files were floor acceleration, inter-storey drift and the base isolator ductility demand, the mean and standard deviation was then calculated and the Probability of Exceedence for different limits and return periods. Thus allows for comparison between the 3 main structural models, the un-isolated structure with shifted mass and no base isolation, a structure with no mass shift but with a base isolator and finally a structure with both shifted mass and a base isolator.

7.1 Effects of Mass Irregularity on a Normal Structure

The effect on mass shift on a normal structure is to affect the periods of free vibration. This can easily be shown in a single degree of freedom structure, where the only variables are the mass of the structure and the stiffness of the elements. The equation for a single degree of freedom structure is

$$T = 2\pi\sqrt{\frac{M}{K}}$$

where T is the period, M is the mass and K is the stiffness. From this it can be seen straight away that for a mass increase the period increases as well. This is beneficial for most structures as it shifts the period of the structure away from the high accelerations of the Acceleration Spectra. This is offset somewhat by the fact that in order to shift the period either the stiffness or the mass must change. It is somewhat easier to affect the stiffness of the elements as a design engineer; however there are often limitations to the change of the stiffness of a structure as it can compromise the safety and/or performance of the structure. The problem of increasing the mass is that even though there is decrease in the acceleration it may not be enough to offset the increase of force due to the increase in mass. This is where base isolation comes into effect as it can adjust the stiffness of the structure without compromising

the safety, also, it does not increase mass of the structure so if the design is done correctly there will be a significant decrease in the acceleration response.

For the multi-degree of freedom structure, this is not as straight forward; this is because the fundamental period is affected by the location of the mass as well as its size. Thus the period can be increased either through an increase or decrease by increasing a mass at a single location, thus the determination of the effects of mass irregularities may be difficult.

For a fixed based cantilever structure it can be generalised that by reducing the height of the overall centre of mass the period of free vibration of the structure will reduce. This is because of the fundamental mode shape is part of the equation, and the more that part of the structure is moving, the more it contributes to the mode. Thus, as the mass is moved upwards in a structure, more of the Mass Participates in the first mode and the longer the period becomes. As with increasing the total mass, the period is increased, but it may be that the accelerations and the shear forces are increased rather than decreased. As before, an extensive check would need to be done to ensure that this is the case.

For base isolated structures, there is a significant effect of the base isolator on the modes of free vibration of the structure. This is because of the initial shift of the base, which means that the first period now dominates most of the response of the structure; this means that the higher modes do not affect the response of the structure as much as for an un-isolated structure. This thesis is looking at how the mass distribution affects the response of the structure.

Figure 7.2 shows how the effect of a mass irregularity affects the fundamental period of an un-isolated structure, and Figure 7.3 shows the mass irregularity affects a based isolated structure. Note that these are based on a structure with the same total mass and stiffness. As it can be seen there is a significant period shift when the mass is concentrated higher in the structure and a reduction in the period, however the magnitude is smaller for the base isolated structure. For higher modes this is not

as straight forward as the locations of the modal nodes are different and thus the effect of the mass irregularity influences the overall response is more complex way.

The first two plots show that the mass irregularity has a similar effect, but there is a slight decrease in the change and the location of the 0% has shifted so that the curve is “stretched”. The difference in the second period is more noticeable as the flexibility of the base isolator means that the mode shapes are different from these of an un-isolated structure as the deformation of the isolator means that often the ground floor level has the maximum model displacement, implying the worst place for the mass irregularity is the base. However this said, the higher modes have a reduced effect when using base isolation.

The period change corresponds to the mode shape. For example; if the mode shape is scaled so that the maximum magnitude is 1, and the shifted mass is located at a position where the mode shape magnitude is close to 1 then there is an increase in the period, and when the shifted mass is located at the at a point of zero modal displacement, then there is a decrease in the period.

From Figure 7.4 and Figure 7.5 it can be seen how the mass shift affects the second natural period of the structure, it is most notable that for a Fixed Base cantilever that there are two points of zero modal displacement, where as for the base isolated structure there is only one. It should also be noted that for the for the second mode that if the building is stiff compared to the base isolator, in terms of overall deformation rather than as a floor by floor basis, then the flexibility of the isolator will dominate the structure. Thus, for a building where the superstructure undergoes a displacement that is twice as large as the base isolator, then the second mode has two points where the modal displacement is 1 or close to 1. This means that there is a large response of the mass in the 2^{nd} mode.

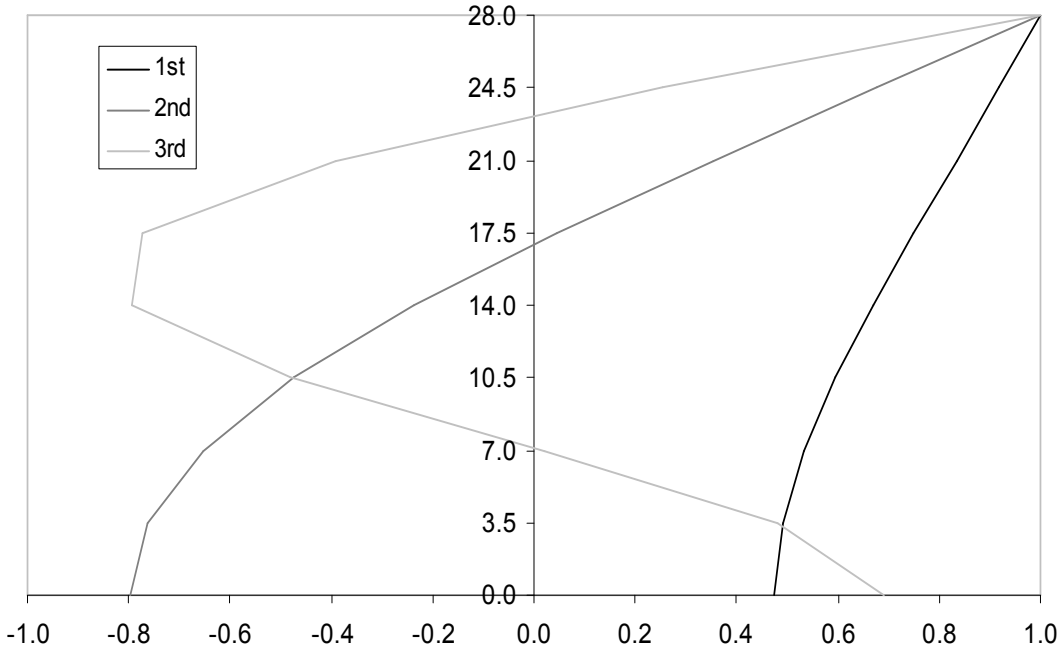

Figure 7.1 Plot of the first three mode shapes for a base isolated structure

The above graph shows that approximately half of the first mode displacement is provided by the isolator displacement and that for the second mode that the base isolator provides significant displacement in the opposite direction to that of the top floor.

Looking at the modal analysis for period of the structure using the mass and stiffness matrices, and the corresponding mode shape can be used to calculate the period, thus it can be used to show how changes to the mode shape affects the result for the natural period. This method is based on using an idealised single degree of freedom structure. The mode shapes are used to normalise the stiffness and mass matrices into a single value, the period that is obtained using these two values is the period corresponding to the mode number, hence in order to obtain the fundamental Period then the first Mode is used. The following equations are used in the calculations

$$m_i^* = \{\phi_i\}^T [M] \{\phi_i\}$$

$$k_i^* = \{\phi_i\}^T [K] \{\phi_i\}$$

$$T_i = 2\pi\sqrt{\frac{m_i *}{k_i *}}$$

For a simple shear stick structure, which only has lateral mass and stiffness the corresponding matrices are relatively straight forward with the mass having only values on the diagonal and the stiffness matrix having a narrow diagonal band, by using the mode shape to obtain a modal mass and stiffness the modal period can be obtained. Thus using the following equations

$$M = \begin{bmatrix} m_1 & & & & & & & \\ & m_2 & & & & & & \\ & & m_3 & & & & & \\ & & & m_4 & \ddots & & & \\ & & & & \ddots & & & \\ & & & & & m_{n-1} & & \\ & & & & & & m_n & \end{bmatrix}$$

$$K = \begin{bmatrix} k & -k & & & & & & \\ -k & 2k & -k & & & & & \\ & -k & 2k & -k & & & & \\ & & -k & 2k & -k & & & \\ & & & -k & \ddots & \ddots & & \\ & & & & \ddots & \ddots & -k & \\ & & & & & -k & 2k & -k \\ & & & & & & -k & 2k \end{bmatrix}$$

and

$$\phi = \{\varphi_1, \varphi_2, \varphi_3, \varphi_4, \ldots, \varphi_{n-1}, \varphi_n\}$$

If the mass and stiffness is constant then $m* = \{\phi\}^T [M] \{\phi\}$ and $k* = \{\phi\}^T [K] \{\phi\}$ become

$$m^* = m\left(\varphi_1^2 + \varphi_2^2 + \varphi_3^2 + \varphi_4^2 + \ldots + \varphi_{n-1}^2 + \varphi_n^2\right)$$

$$m^* = m\sum_{i=1}^{n} \varphi_i^2$$

$$k^* = k\left(\varphi_1^2 + 2\varphi_2^2 + 2\varphi_3^2 + 2\varphi_4^2 + \ldots + 2\varphi_{n-1}^2 + 2\varphi_n^2\right)$$
$$- 2k\left(\varphi_1\varphi_2 + \varphi_2\varphi_3 + \varphi_3\varphi_4 + \ldots + \varphi_{n-2}\varphi_{n-1} + \varphi_{n-1}\varphi_n\right)$$

$$k^* = k\varphi_1^2 + k\sum_{i=2}^{n} \varphi_i^2 - 2k\sum_{i=1}^{n-1} \varphi_i\varphi_{i+1}$$

$$k^* = k\left(\varphi_1^2 + 2\sum_{i=2}^{n} \varphi_i^2 - 2\sum_{i=1}^{n-1} \varphi_i\varphi_{i+1}\right)$$

$$T = 2\pi\sqrt{\frac{m^*}{k^*}}$$

$$T = 2\pi\sqrt{\frac{m}{k}\frac{\sum_{i=1}^{n} \varphi_i^2}{\left(\varphi_1^2 + 2\sum_{i=2}^{n} \varphi_i^2 - 2\sum_{i=1}^{n-1} \varphi_i\varphi_{i+1}\right)}}$$

For a Flexural Structure, the mass matrix is similar to that of a shear structure; however, the stiffness matrix becomes more complex due to the interaction of the rotation of the nodes and their deflection. In Appendix A: Modal Analysis (Analytical) a similar model is developed for Shear and Flexural structures based on the assumption that the mass is uniform up the structure, so thus it is valid for tall structures. The equations can used to obtain an estimate of the fundamental period for short buildings; however this value is not accurate and must be further checked through additional calculations.

There are other useful equations from Appendix A: Modal Analysis (Analytical) is the effective height and effective mass of the modal periods. These equations can help as they can be used to estimate the effect of any mass irregularities that occur off of a uniform mass distribution.

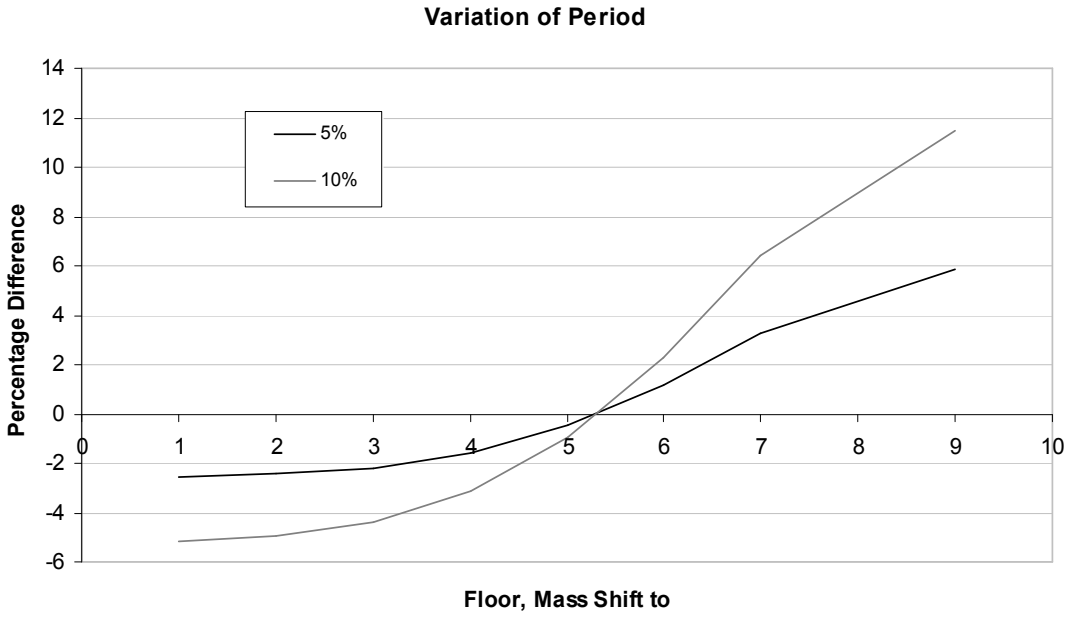

Figure 7.2 Plot showing the variation of fundamental period for an un-isolated structure, the floor indicates the location of mass irregularity

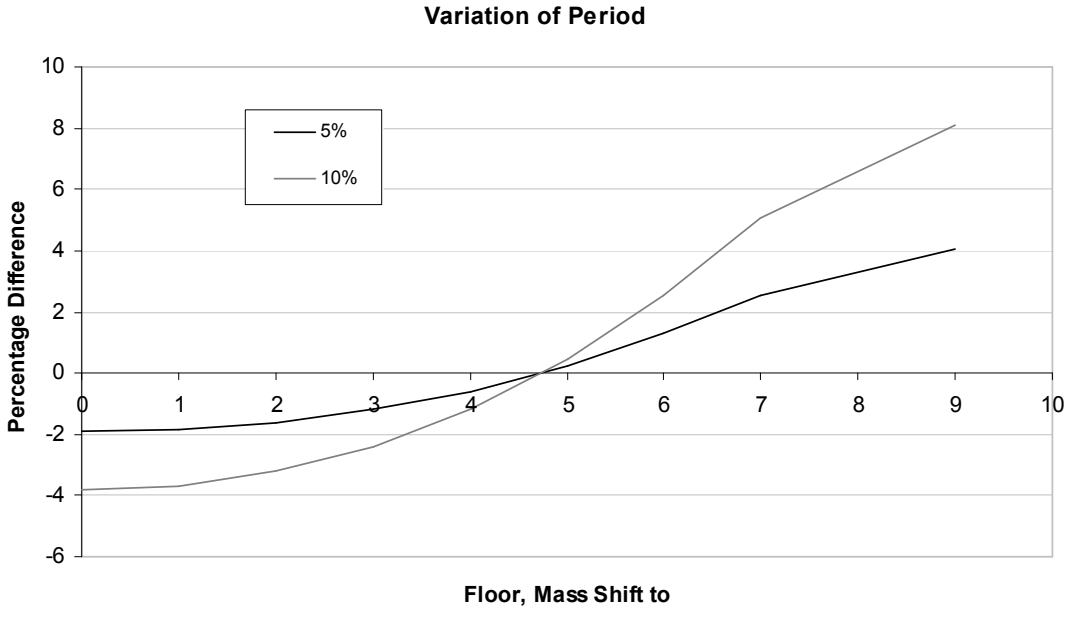

Figure 7.3 Plot showing the variation of fundamental period for a base isolated structure, the floor indicates the location of mass irregularity

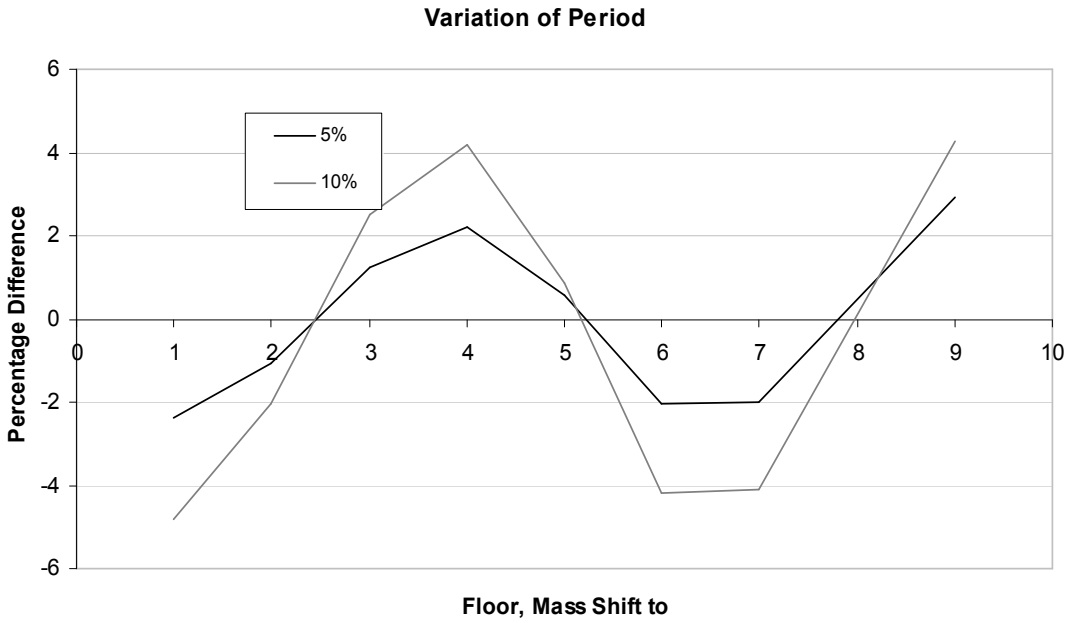

Figure 7.4 Plot showing the variation of second period for an un-isolated structure, the floor indicates the location of the mass irregularity

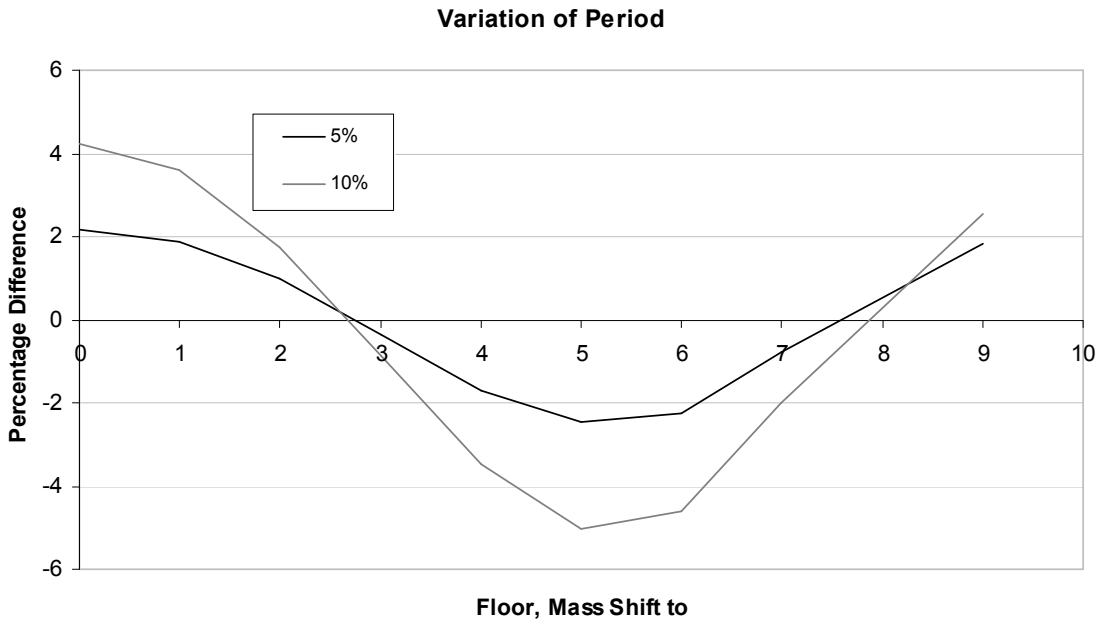

Figure 7.5 Plot showing the variation of the second period for a base isolated structure, the floor indicates the location of the mass irregularity

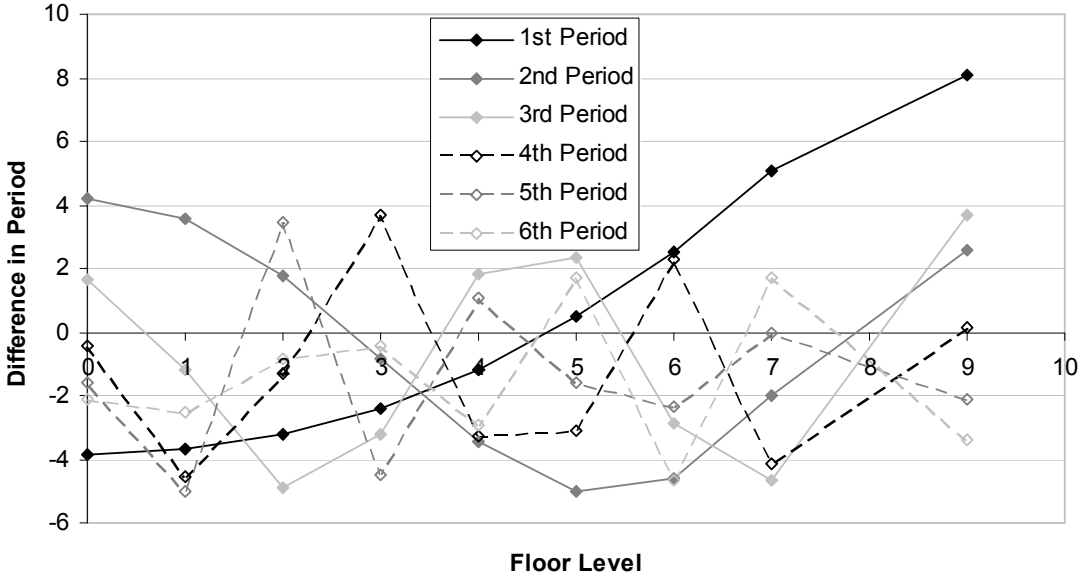

Figure 7.6 Plot showing the variation of period for the first six modes (for initial stiffness of the base isolator)

From Figure 7.6 it can be noted that there is no location that the mass irregularity can occur which does not increase one of the modal periods of the structure. The objective is to minimize the total effect of the mass irregularity. The main choice is to decide where to place the shifted mass for best overall period increase. An increase in period is equivalent to a more flexible structure, and thus smaller accelerations. This is where the use of the effective mass comes in, the effective mass is an indicator how much of the mass is being excited by a particular mode, and the effective mass summed over all modes and is equal to the total mass.

Figure 7.7 shows the percentage effective mass that each mode attracts of the total mass. For an un-isolated structure the first mode attracts approximately 65.1% while the second mode attracts approximately 20.1%. If the initial stiffness of the base isolator is equal to the stiffness of the structures then the first mode attracts 86.0% and the second mode attracts 13.9% of the total mass. If the base isolator yields then the first period effective mass is 99.85% of the total mass and the second mode attracts the remaining 0.15%. This means that the response of the structure is

dominated by the fundamental mode for base isolated structures especially once the base isolator yields.

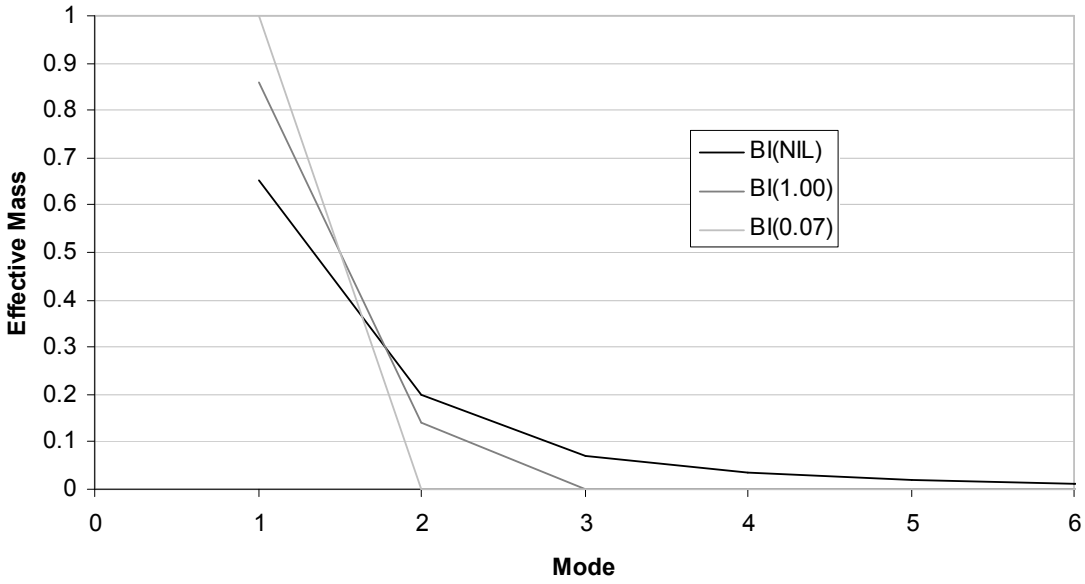

Figure 7.7 Plot showing the Effective Mass of each Mode, the value in the brackets indicates the ratio of Base Isolation Stiffness used in the Calculations and Designed Stiffness

7.2 Effects of Base Isolator Stiffness and Yield Capacity

The effects of the Base Isolator parameters on the response of the structure should be noted, as by changing the stiffness of the isolator or its yielding strength can greatly affect the peak response of the structure. It can be seen in the two parameters form four different variations, which differentiates the response of the structure into four distinct bands. It should be noted that by increasing the flexibility of the isolator that the response of the structure is less severe and that increasing the yield strength of the Isolator increases the Probability of Exceedence for Acceleration and Drift limits.

Effects of Mass Shift on Floor Acceleration

Figure 7.8, Figure 7.9 and Figure 7.10 all show the Probability of Excedence of the roof Acceleration, the difference being where the mass shift is located. For Figure 7.8 it is on the ground floor, for Figure 7.9 the mass shift is located midway up the structure and for Figure 7.10 the mass shift is located on the top (roof level) of the structure. Observing the results along with Figure 7.3 the effect of mass shift can be further noted that with the shifted mass on the bottom floor, that the decrease in the natural period, and hence increase in the stiffness and base shear coefficient that there is a lesser effect then with the shifted mass at halfway up the Structure. This is due to there being little change in the natural period of the structure when the shifted mass is located near the mid height of the structure. When the Mass is located at the top of the structure, there is an increase in the natural period and hence a decrease in the stiffness and base shear. This is due to the effect of the mass shift affecting the effective stiffness of the structure rather than that shown in Figure 7.8, where the mass is essentially removed by the being located on the bottom floor. It should be noted that there is banding of the results for the different structures. This is through the initial stiffness, yielded stiffness and the yield strength of the base Isolation unit.

For the following figures, the numbers for the lines are coded to give the percentage of mass shifted, the floor the shifted mass is located, the yield strength of the Isolator as a percentage of the total structural weight and the initial and post yield stiffness of

the Isolator. Reading from right to left the first 2 digits are the post yield period (hence stiffness) of base isolator, the third and fourth are the initial period of the base isolator, the fifth and sixth are the yield strength of the isolator as a percentage of total weight of the structure. The seventh digit is the location of the shifted mass, the last digit or 2 digits are the shifted mass, as a percentage of the total mass.

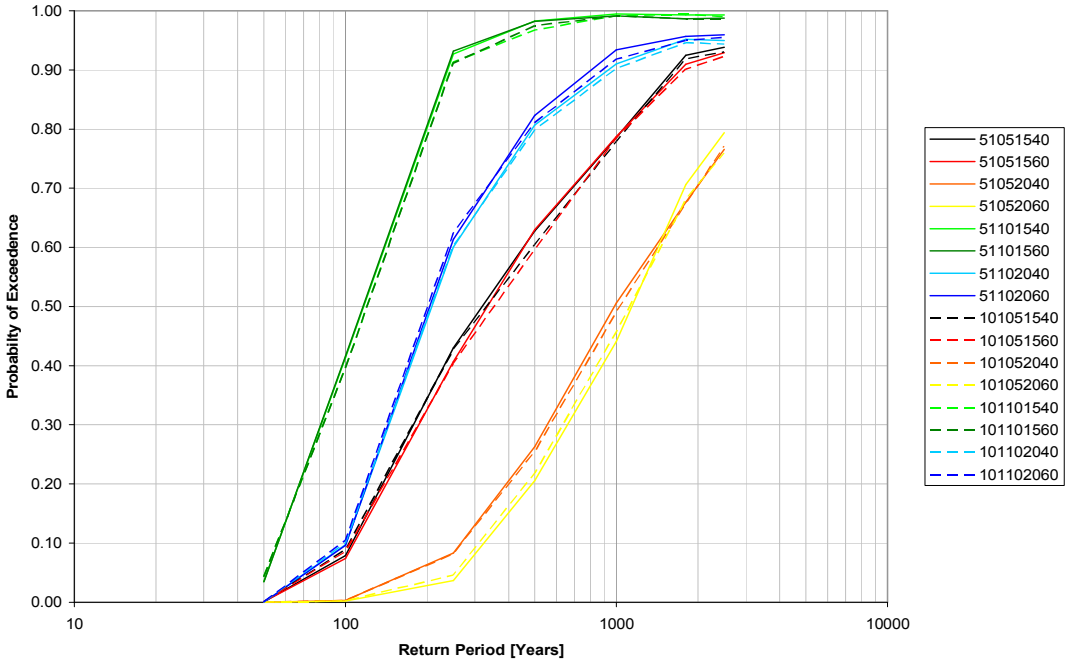

Figure 7.8 Plot of roof accelerations for a structure with the mass irregularity located on the bottom level. Note: Solid lines are for isolator a yield strength equal to 5% of the seismic weight and the dashed lines are for a yield strength of 10%

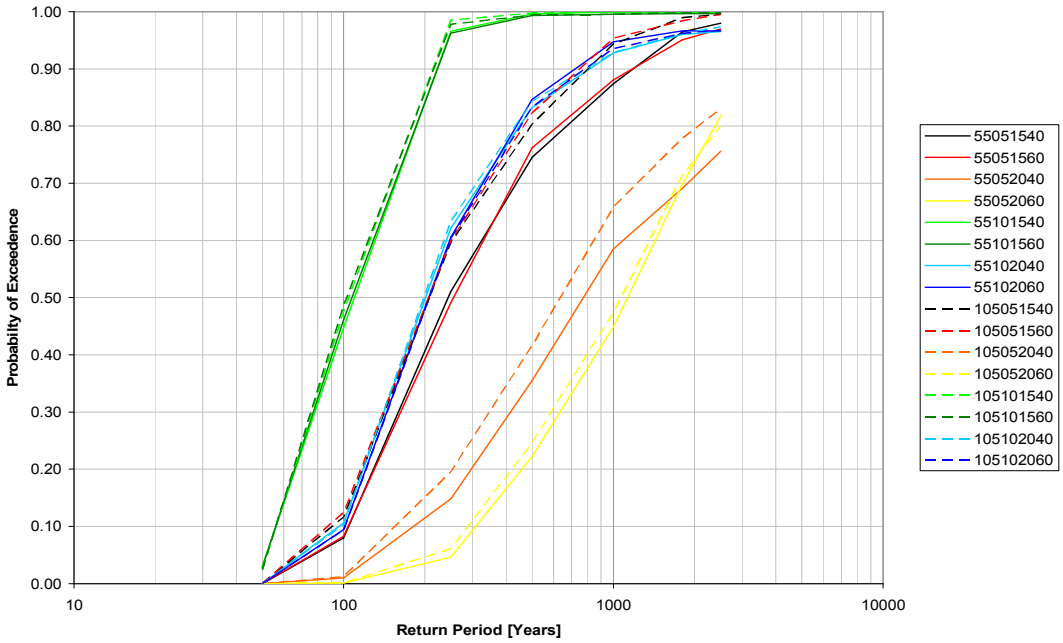

Figure 7.9 Plot of roof accelerations for a structure with the mass irregularity located on the 5th level. Note: Solid lines are for isolator a yield strength equal to 5% of the seismic weight and the dashed lines are for a yield strength of 10%

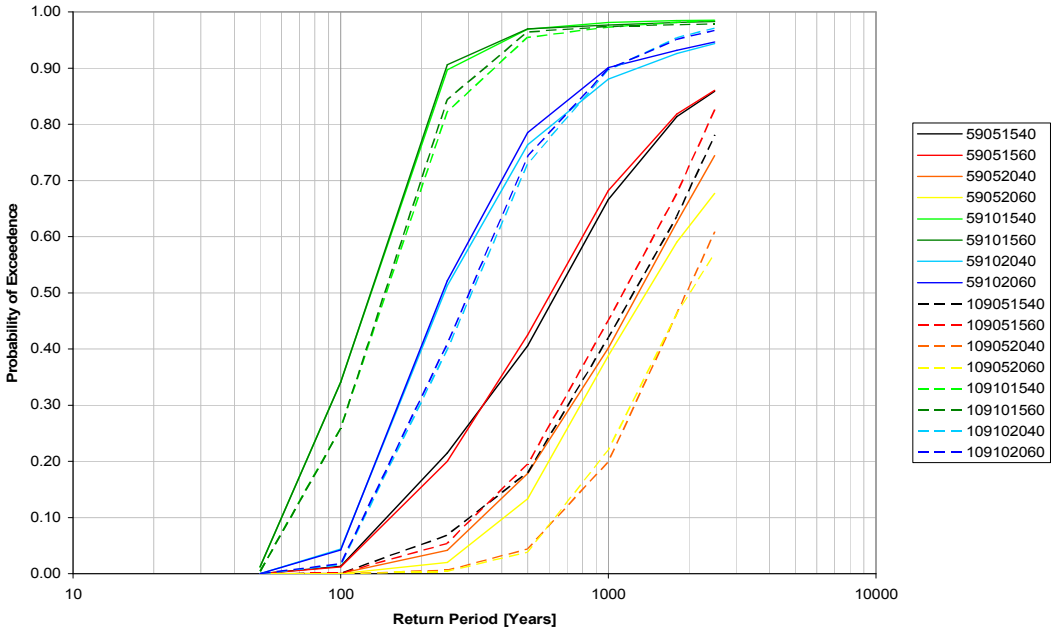

Figure 7.10 Plot of roof accelerations for a structure with the mass irregularity located on the roof level. Note: Solid lines are for isolator a yield strength equal to 5% of the seismic weight and the dashed lines are for a yield strength of 10%

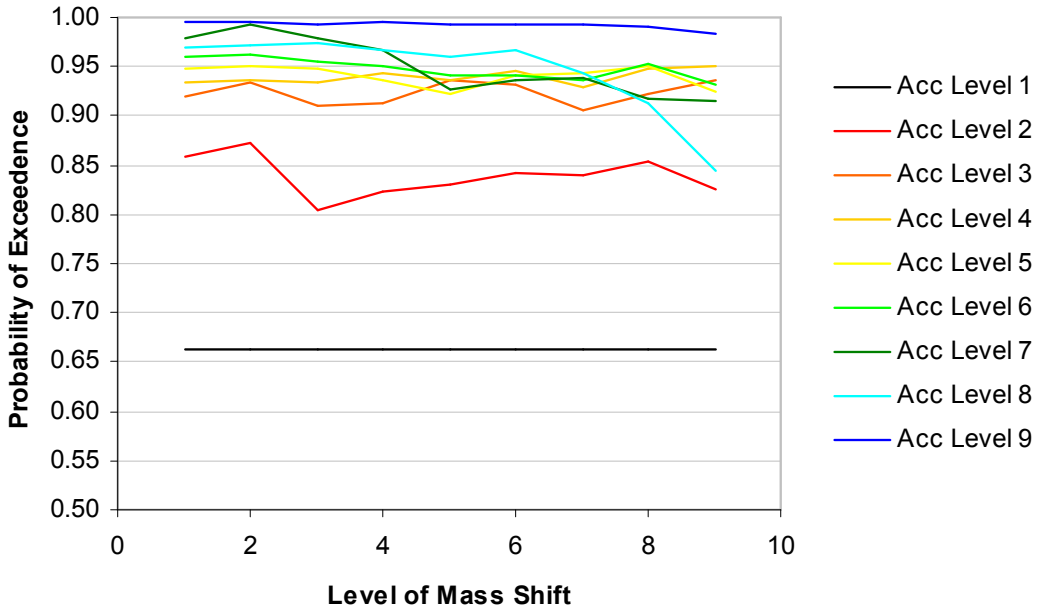

Figure 7.11 Plot of Probability of Exceedence for the return period of 250 years. The data is showing the effect of mass irregularity on the response of a structure for each floor but with the mass irregularity at different locations.

Figure 7.11 shows the effect of the mass irregularity for each floor with the location of the mass irregularity as the independent variable. The plot shows that as the mass shifts up the structure that there is a trend for the floor acceleration to decrease. Note; level 1 did not experience a variation due to the model having the bottom floor directly connected to the earthquake excitation.

Effects of Mass Shift on Inter-storey Drifts

Inter-storey drifts have been used to calculate expected damage to the structure during earthquake events. There have been numerous methods for estimating the damage, which include methods such as taking the maximum and minimum inter-storey drifts achieved, a weighted average of the maximum and minimum inter-storey drifts, and others that require the full time history of the element to determine the incremental damage caused.

The model for the un-isolated structure was run with the results plotted in

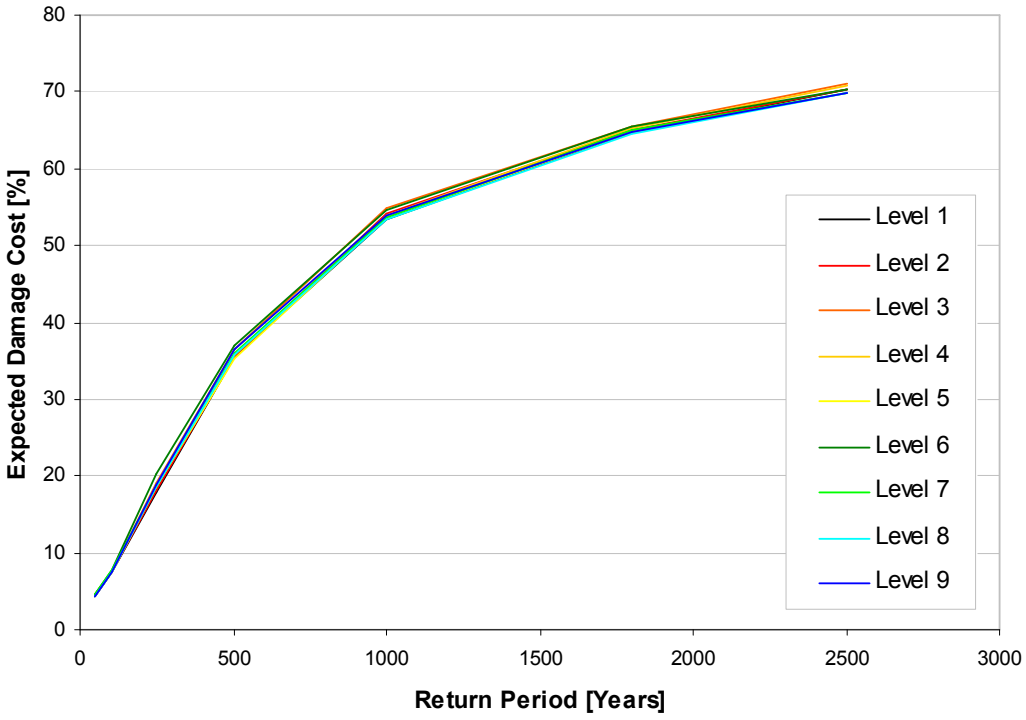

Figure 7.12 and Figure 7.13, these show how the roof level is affected by the mass location on the different floors and for the 2 different shift masses, 5% and 10% of total mass was relocated for the two different structures.

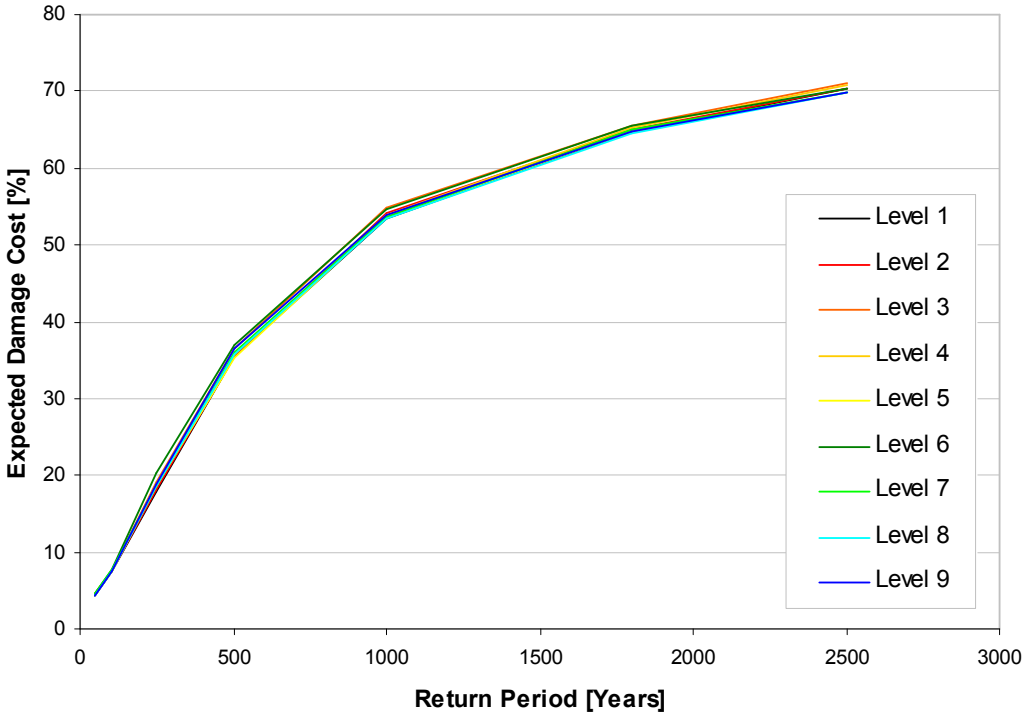

Figure 7.12 Expected damage cost for inter-storey drift on top level for a 5% mass shift different floor levels. This is for an un-isolated structure

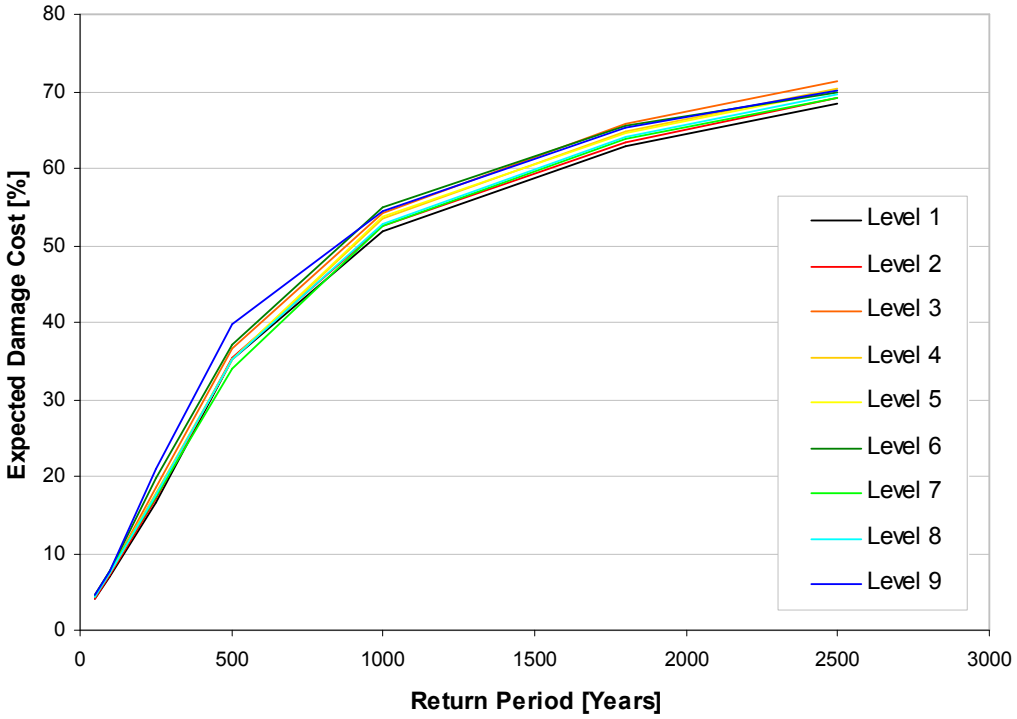

Figure 7.13 Expected damage cost for inter-storey drift on top level with a 10% mass shift different floor levels. This is for an un-isolated structure

Note that the having the shifted mass further up the structure causes the structure to become more flexible and hence have larger inter-storey drift demands. The two graphs show how the mass shift affects the response, as the mass shift moves up the strucutre, the upper and lower limits move outwards. For the 5% mass shift, the responses are less spread out then the responses are for the 10%. This means that for small irregularities within the structure, there is no real problem in the changed response of the structure, however for large shifts, such as for large machinery or plant, there may need to be a serious redesign for the entire structure, not just immediate and supporting components. It should be noted that the increase in the Expected Damage index is affected by the return period of the earthquake. For the frequent but low amplitude earthquakes, there is little variation, however for high amplitude earthquakes there is significant variation within the response, which is due to the fundamental period of the structure as the effects of the shifted mass become more pronounced and causes the structure to underground larger drift demands.

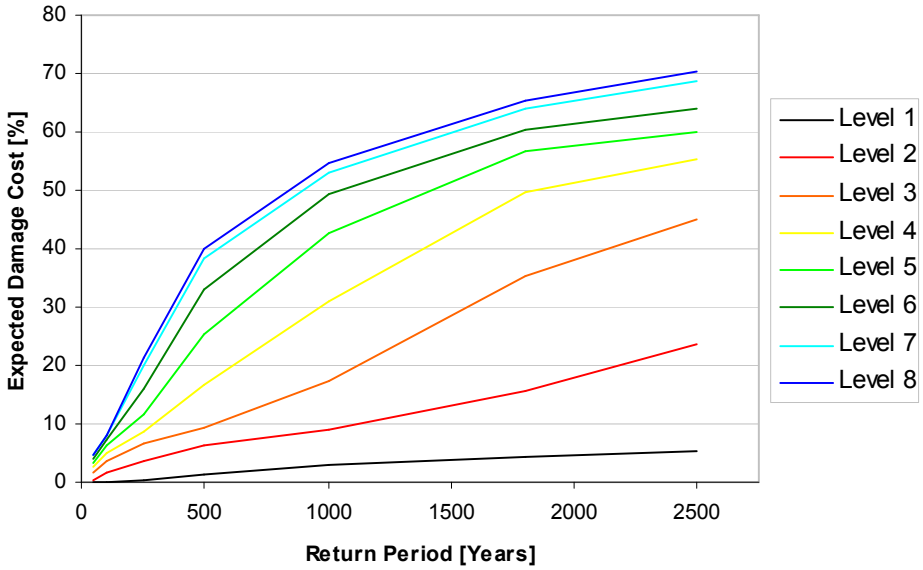

Figure 7.14 Plot of expected damage cost due to drift for a structure with 10% of the total mass shifted to the highest level in the structure. This structure is un-isolated, and the level refers to the inter-storey drift level

The expected damage caused to the structure due to an earthquake excitation is shown in Figure 7.14 when there is a 10% mass is shift to the roof level. From the figures there is severe damage occurring to the higher levels. The expected damage increases with floor level and return period. This is due to the increase in the base earthquake excitation as the earthquakes are scaled larger in magnitude as specified in NZS 1170.5 (Standards New Zealand. 2004).

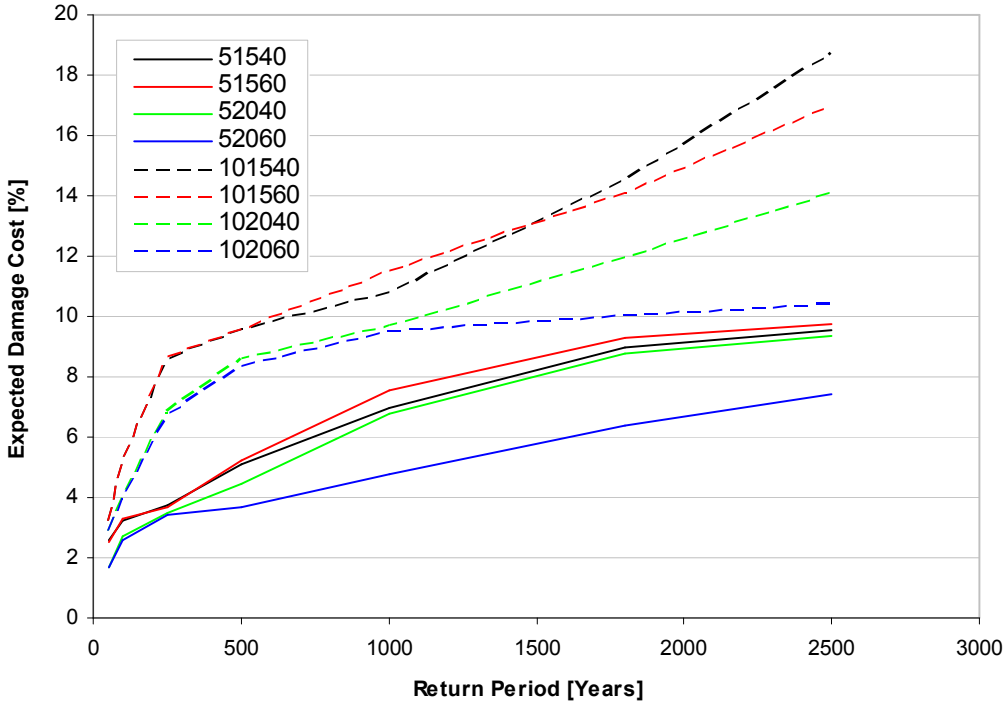

Figure 7.15 Plot of expected damage costs for inter-storey drift of the top level for the different variations of the isolator unit. There is no shifted mass within the structure

The effect of doubling the yield strength of the isolator can be seen to approximately double the expected damage of the structure, as seen in Figure 7.15. This is an expected response as by doubling the strength of the isolation unit means that approximately double the forces that are transmitted through the isolator to the structure, and hence give an increased response.

A comparison of Figure 7.16 and Figure 7.18 shows how the shifting of the mass from the bottom floor to the top floor can dramatically affect the response of the structure. The effect of the shifted mass being brought down to the bottom of the structure caused a slight stiffness increase, hence shorter oscillation amplitudes and thus smaller inter-storey drifts at higher levels. Also the mass shift does not significantly affect the response of the structure when the mass shift occurs in the lower levels of the structure. The largest change to the structural response occurs when the mass shift occurs at the highest level.

Figure 7.18 shows a plot of the expected damage cost due to the inter-storey drift between 8th and 9th levels. It should be noted that the structural difference between the lines are mass shift location and whether an Isolation unit is present, this means that the plot is showing both how base isolation effects the response of the mass shift and how the mass shift effects the response of a base isolated structure. Figure 7.18 shows that having an isolated structure over an un-isolated structure can greatly reduce the expected damage to the structure, however, care must be taken if there is any large structural abdominally, such as stiffness or mass change, due to the possibility of adverse responses from the structure.

Figure 7.16 Plot of expected damage costs due to inter-storey drift for the configuration of a 10% mass shift to the bottom level and an isolator yield strength of 5%, an initial period of 1.5s and a post yield period of 4.0s

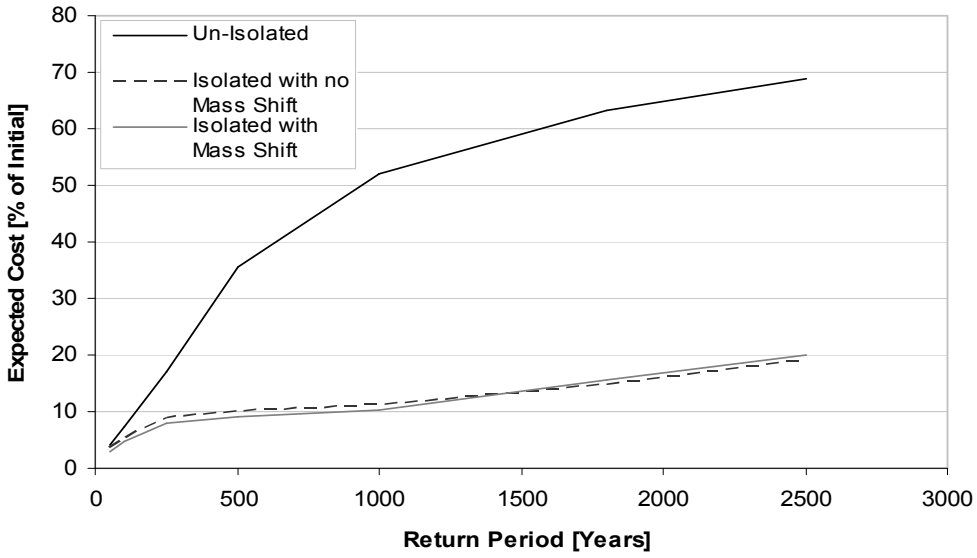

Figure 7.17 Plot of expected damage costs due to inter-storey drift for the configuration of a 10% mass shift to the bottom level and an isolator yield strength of 10%, an initial period of 1.5s and a post yield period of 4.0s

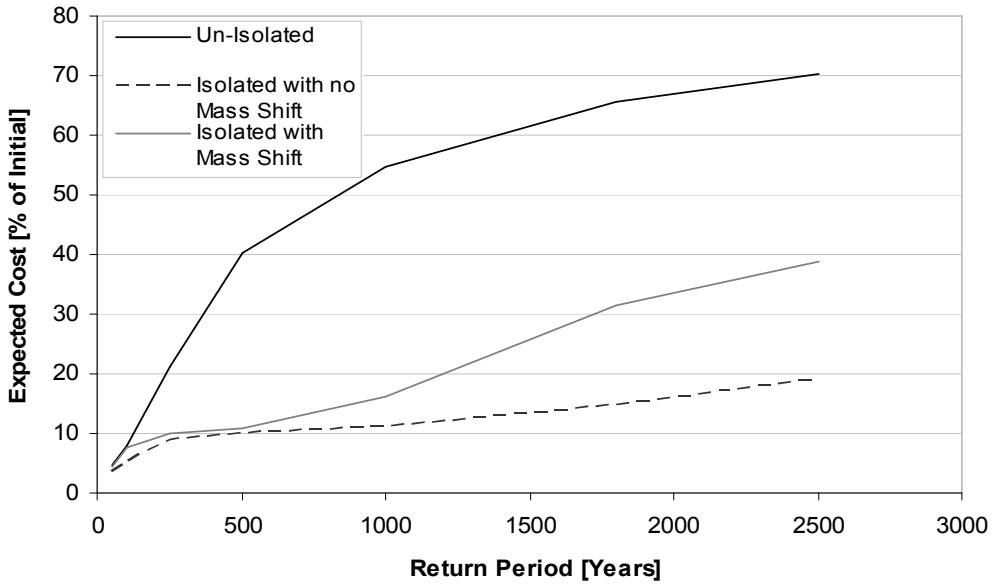

Figure 7.18 Plot of expected damage costs due to inter-storey drift for the configuration of a 10% mass shift to the roof level and an isolator yield strength of 10%, an initial period of 1.5s and a post yield period of 4.0s

7.3 *Ductility of Base Isolation Unit*

Figure 7.19 show the results for the Base Isolated structure without any mass shifts, the main part which they show is the exhibit definite banding for the both the yield strength and initial stiffness of the base isolation unit. Figure 7.20 also shows the data as Figure 7.19. However, it is in terms of the non-linear factor, which indicates how well it compares to a perfectly rectangular hysteretic loop. It can be seen that the higher ductility demands on the base isolation units causes the efficiency of the unit to become less optimal, it should be noted that the difference of the lines is due to the higher yield strength; the yield strength affects the non-linear factors from the analyses due to there being a smaller ductility demand for a given return period, hence there needs to be a larger excitation in order for the base isolation unit to reach its full potential, this is significantly shown in Figure 7.20.

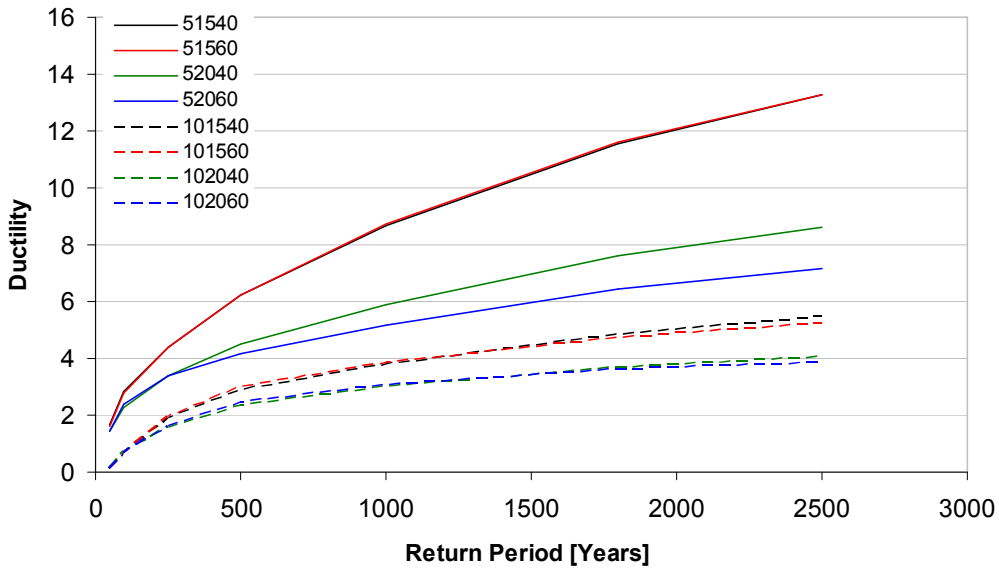

Figure 7.19 Average maximum ductility of the base isolation unit during earthquake excitation with no mass irregularities

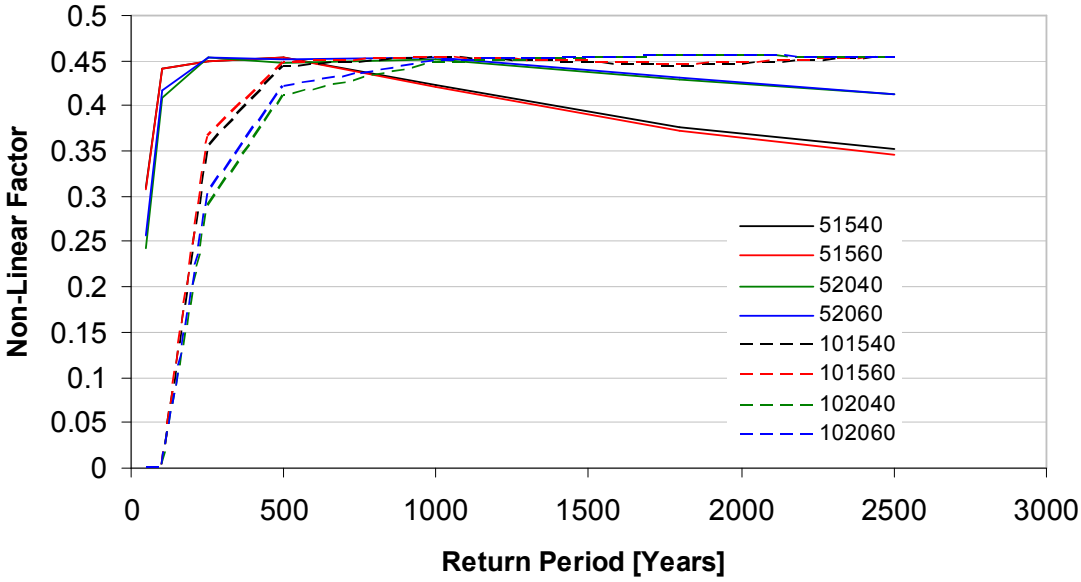

Figure 7.20 Average maximum non-linearity of the base isolation unit during earthquake excitation

Figure 7.21 and Figure 7.22 show the ductility demand of the Isolator when there is a 10% mass shift, located on the bottom level and roof level respectively. From the two figures it can be noted that the mass shift has little effect on the ductility demand of the isolator. When Figure 7.21 and Figure 7.22 are compared to Figure 7.19 there is still little difference in the ductility demand of the Isolator unit, this further emphasising that the location of the mass has little effect on the ductility. The size of the mass shift was 10%, based on previous results of the effect of the size of mass shift on the floor acceleration and inter-storey drift, then it is possible to say that the 5% mass shift will less effect then the 10% mass shift and will not be commented on further in this section.

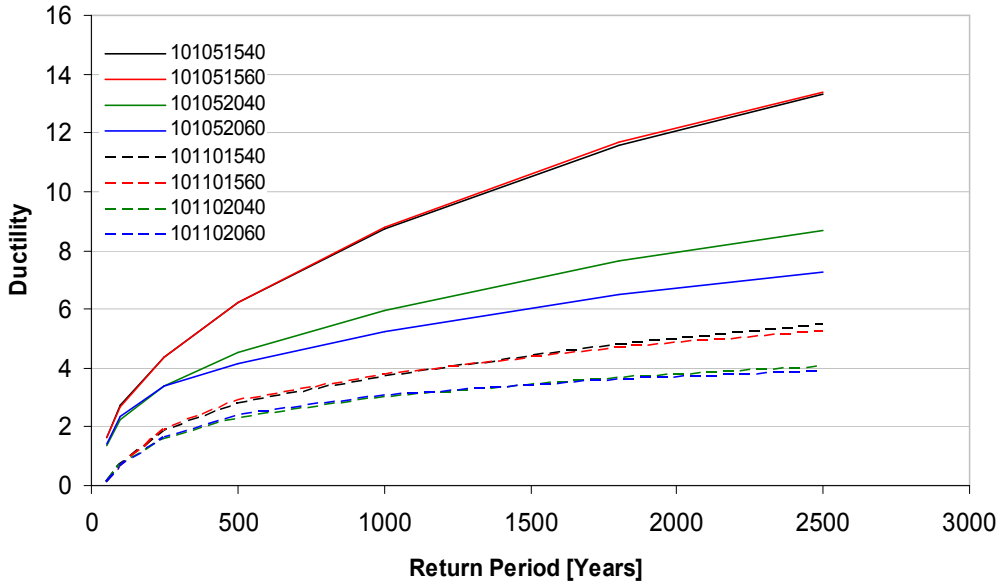

Figure 7.21 Average maximum ductility of the base Isolation unit during earthquake excitation, the structure has a 10% mass shift located on the bottom level

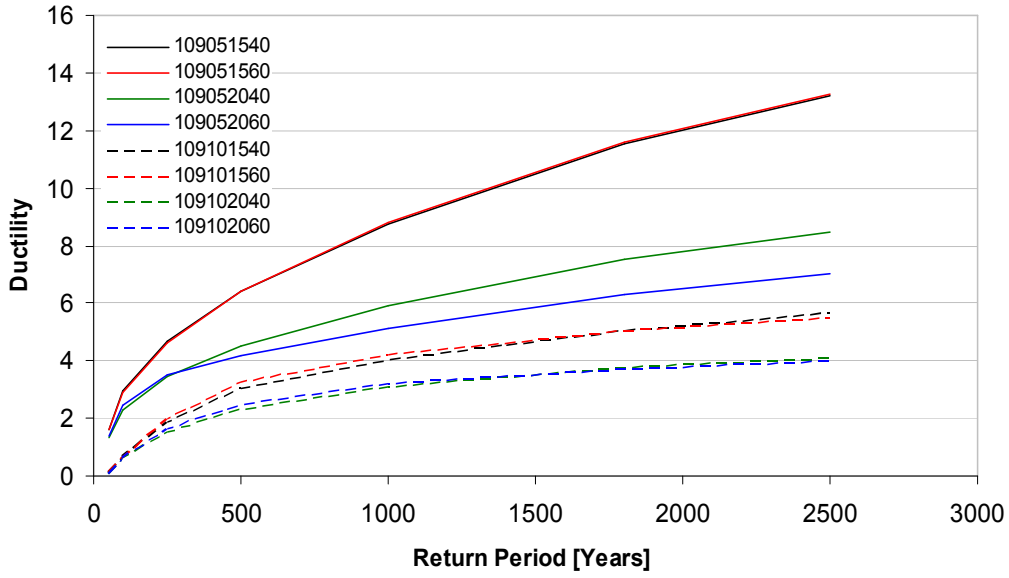

Figure 7.22 Average maximum ductility of the base isolation unit during earthquake excitation, the structure has a 10% mass shift located on the roof level

8 Discussion and Conclusions

The results from the analysis of the 8 storey structure shows how the main effect of base isolation is to greatly reduce the damage due to inter-storey drift and the affects of natural period change on floor acceleration. The drift was converted to expected damage costs allowing for a comparison between the base isolated and un-isolated structures, which show that, as expected there was a significant decrease in the costs associated with a seismic excitation. It should also be noted that superstructure with no mass shift on a base isolator gave a better response then a superstructure with a mass shift; this is most evident in Figure 7.18 where the data is collected from the top floor inter-storey drift. The floor acceleration was used to show how the structure responded to the mass shifts and base isolation; this is to shown because while inter-storey drifts are indicative of structural damage, floor acceleration is the cause of movement of and damage to non-structural items such as furniture, equipment and people.

The ductility of the base isolator was also considered as part of the analysis to observe how much demand is put onto the isolator due to the structural variations, and differing isolator variations. The main observation for the isolator units was that the yield strength of the isolator was the main influence on the response of the structure with the initial stiffness second most important variable. The post yield stiffness had little impact on the structural response compared to the above two characteristics. This is most notable in Figure 7.20 which presents the two significant bandings. It should be noted that the effect of the mass shift had little to no effect on the ductility demand of the structure.

From several aspects on the analysis it can be concluded that the yield strength of the isolator is the main factor affecting the response of the structure, the effects of initial isolator stiffness can greatly influence the response of the structure as well. The yield strength affects the acceleration by controlling how much energy can be transferred through the isolator unit by hysteretic behaviour. The initial stiffness can further affect the acceleration by changing the fundamental period of the entire structure, it should be noted that by increasing the period of the structure reduces

accelerations; however this can be at the cost of higher displacements and thus higher inter-storey drifts. The data from the analyses show that increasing the initial period of the base isolation units reduced the ductility demand of the isolators, while for the structure increasing the effective height of the mass, hence a longer fundamental period, with the result that the structure experienced a higher inter-storey drift demand which was most notable at the top floor.

The effect of the mass shift within the structure is to increase the natural period of free vibration and thus reducing the floor accelerations of the top floor level. In the case of inter-storey drift, for an un-isolated structure, there is an increase in the expected damage incurred during the event as the structure has become less stiff and hence deforms more. This is more pronounced when the mass shift is larger as there is a greater change in the effective stiffness. This only occurs when the mass is shift upwards within the structure. Moving the mass shift to the bottom of the structure does not change the effective stiffness, however the reduction in the floor acceleration is not as large.

For an un-isolated structure the effect of mass shift is to reduce the effective stiffness when the mass shift is above the 5^{th} floor and there is an increase in the effective stiffness when the mass shift is below the 5^{th} floor. This is because as the shifted mass is located below the effective height of the structure and it is effectively being removed from the structure and at the limit, when the mass is at ground level; the mass is completely removed from the equations as the ground level is fixed. This is not true for base isolated structures as the equations no longer treat the ground floor as fixed in the horizontal direction, however the analyses has shown that there is still a noticeable difference in the expected damage costs due to inter-storey drifts.

9 Recommendations

For the best use of base isolation in terms of drift demand on a structure ensuring that any large mass irregularities are located towards the bottom of a structure helps to reduce the maximum drift demand on the structure. The change in drift has a corresponding stiffness increase, hence higher accelerations. however, these accelerations are not severe but should be taken in to account, especially if the structure is already near design capacity.

When designing an isolator unit using a lower initial stiffness greatly reduces both the drift and floor acceleration demands on the structure. This is matched by requiring that the isolator undergoes larger deformations and as such should be taken into account when designing structures that have restrictions on allowable movement. The magnitude of the mass irregularity can be used to the advantage of the Designer, depending on the location that it occurs. If the mass irregularity is located below the effective height of the fundamental period then there will be a more significant decrease in the drift demand on the structure, while there is a larger increase in the floor accelerations.

10 Suggestions for Future Research

Suggestions for further research would be to look at the effects of mass shifts for both isolated and un-isolated shear structures or frame structures as the maximum drift demand is near the bottom of the structure rather then the top. This thesis looked only at a flexural structure, or wall structure.

A study could examine more closely at the effects of the higher level modes within the response of the structure. It should be noted that some research has been done on this already (Skinner, Robinson et al. 1993).

A study also needs to examine at the effects of base isolation units during events that far exceed their design excitation, such as in the case of a base isolator designed for a 500 year return period earthquake, but then subjected to a 2500 year earthquake.

References

Alhan, C. and H. P. Gavin (2005). "Reliability of base isolation for the protection of critical equipment from earthquake hazards." Engineering Structures **27**(9): 1435-1449.

Andriono, T., A. J. Carr, et al. (1990). Seismic resistant design of base isolated multistorey structures. Christchurch, N.Z., Dept. of Civil Engineering University of Canterbury.

Carr, A. J. (2005). Ruaumoko Volume 2: User Manual for the 2-Dimensional Version, Ruaumoko2D. Christchurch, N.Z., Dept. of Civil Engineering, University of Canterbury.

Clough, R. W. and J. Penzien (1993). Dynamics of structures. New York, McGraw-Hill.

Elnashai, A. S. and Society of Earthquake and Civil Engineering Dynamics. (1995). European Seismic Design Practice : research and application : proceedings of the Fifth SECED Conference on European Seismic Design Practice, Chester, United Kingdom, 26-27 October 1995. Rotterdam ; Brookfield, A.A. Balkema.

Foltz, R. (2004). "Estimating Seismic Damage and Repair Costs."

Grant, D. N., G. L. Fenves, et al. (2005). Modelling and analysis of high-damping rubber bearings for the seismic protection of bridges. Pavia, Italy, IUSS Press.

Hong, W.-K. and H.-C. Kim (2004). "Performance of a multi-story structure with a resilient-friction base isolation system." Computers & Structures **82**(27): 2271-2283.

Jangid, R. S. (2006). "Optimum lead-rubber isolation bearings for near-fault motions." Engineering Structures **In Press, Corrected Proof**.

McCarthy, D. F. (2002). Essentials of soil mechanics and foundations : basic geotechnics. Upper Saddle River, NJ, Prentice Hall.

Pocanschi, A. and M. C. Phocas (2006). "Earthquake isolator with progressive nonlinear deformability." Engineering Structures **In Press, Corrected Proof**.

Priestley, M. J. N., R. L. Crosbie, et al. (1978). "Seismic Forces in Base Isolated Masonry Structure." Bulletin of the New Zealand National Society for Earthquake Engineering **11**(4): 219-233.

Skinner, R. I., W. H. Robinson, et al. (1993). An introduction to seismic isolation. Chichester ; New York, Wiley.

Standards New Zealand. (2004). Structural design actions. Wellington [N.Z.], Standards New Zealand.

Table of Figures

Appendix A: Modal Analysis (Analytical)

Mode Shapes, Effective Mass and Effective Height

Shear Structure

$$\rho \frac{\partial^2 u}{\partial t^2} = GA_s \frac{\partial^2 u}{\partial x^2}$$

$$u(x,t) = Y(t).\varphi(x)$$
$$\frac{\partial}{\partial x} u(x,t) = Y(t).\varphi'(x)$$
$$\frac{\partial^2}{\partial x^2} u(x,t) = Y(t).\varphi''(x)$$

$$\frac{\partial}{\partial t} u(x,t) = Y'(t).\varphi(x)$$
$$\frac{\partial^2}{\partial x^2} u(x,t) = Y''(t).\varphi(x)$$

$$\frac{\partial^2 u}{\partial x^2} = \frac{\rho}{GA_s} \frac{\partial^2 u}{\partial t^2}$$
$$\frac{\varphi''(x)}{\varphi(x)} = \frac{\rho}{GA_s} \frac{Y''(x)}{Y(x)} \equiv -\phi^2 = -\frac{\rho}{GA_s} \omega^2$$

$$\varphi(x) = C \exp(sx)$$
$$\frac{\partial}{\partial x} \varphi(x) = Cs \exp(sx)$$
$$\frac{\partial^2}{\partial x^2} \varphi(x) = Cs^2 \exp(sx)$$

$$\frac{\varphi''(x)}{\varphi(x)} = -\phi^2$$
$$\frac{Cs^2 \exp(sx)}{C\exp(sx)} = -\phi^2$$
$$(s^2 + \phi^2)C\exp(sx) = 0$$

$$s^2 = -\phi^2$$
$$s = \pm i\phi$$

Hence

$$\varphi(x) = C_1 \exp(i\phi x) + C_2 \exp(-i\phi x)$$

or alternatively

$$\varphi(x) = B_1 \sin(\phi x) + B_2 \cos(\phi x)$$

Boundary Solutions are that deflection at the base equals zero and shear at the top is equal to zero, or

$$\varphi(0) = 0$$
$$\frac{\partial}{\partial x}\varphi(H) = 0$$

$$\varphi(x) = B_1 \sin(\phi x) + B_2 \cos(\phi x)$$
$$\frac{\partial}{\partial x}\varphi(x) = \phi B_1 \cos(\phi x) - \phi B_2 \sin(\phi x)$$

$$\varphi(0) = B_1 \sin(0) + B_2 \cos(0) = B_2 = 0$$
$$\frac{\partial}{\partial x}\varphi(H) = \phi B_1 \cos(\phi H) - \phi B_2 \sin(\phi H) = 0$$

but as $B_2 = 0, B_1$ *must be non zero for a non – trival solution, hence*

$$\cos(\phi H) = 0$$
$$\phi H = \frac{\pi n}{2} \quad for\ n = 1,3,5\ldots$$
$$\phi = \frac{\pi n}{2H} \quad for\ n = 1,3,5\ldots$$

$$\omega^2 = \phi^2 \frac{GA_s}{\rho}$$

$$\omega = \phi \sqrt{\frac{GA_s}{\rho}}$$

$$\omega = \frac{\pi.n}{2.H} \sqrt{\frac{GA_s}{\rho}} \qquad \text{for } n = 1, 3, 5\ldots$$

$$\omega = \frac{\pi.n}{2} \sqrt{\frac{GA_s}{\rho.H^2}} \qquad \text{for } n = 1, 3, 5\ldots$$

$$T = \frac{2\pi}{\omega}$$

$$T = \frac{4}{n} \sqrt{\frac{\rho.H^2}{G.A_s}} \qquad \text{for } n = 1, 3, 5\ldots$$

The Effective Height of the structure of a given displacement shape can be determined using the following equation

$$h_e = \frac{\int_0^H \varphi(x).x.dx}{\int_0^H \varphi(x).dx}$$

Using the mode shapes as the displacements, we can determine the effective height of each mode. This can be used with the Effective Mass in order to determine the over-turning moment produced on the structure for each mode.

$$h_e = \frac{\int_0^H \sin(\phi.x).x.dx}{\int_0^H \sin(\phi.x).dx}$$

$$h_e = \frac{\left[\left(\frac{2.H}{\pi.n}\right)^2 \sin(\frac{\pi.n}{2.H}x)\right]_{x=0}^{H} - \left[\frac{2.H}{\pi.n}x.\cos(\frac{\pi.n}{2.H}x)\right]_{x=0}^{H}}{\left[-\frac{2.H}{\pi.n}\cos(\frac{\pi.n}{2.H}x)\right]_{x=0}^{H}} \qquad \text{for } n = 1, 3, 5\ldots$$

$$h_e = \frac{\left(\frac{2.H}{\pi.n}\right)\left[\sin(\frac{\pi.n}{2}) - 0\right] - \left[H\cos(\frac{\pi.n}{2}) - 0\right]}{-\left[\cos(\frac{\pi.n}{2}) - 1\right]} \qquad \text{for } n = 1, 3, 5\ldots$$

$$h_e = \left(\frac{2.H}{\pi.n}\right)\sin(\frac{\pi.n}{2}) \qquad \text{for } n = 1, 3, 5\ldots$$

Note: the Effective Height of the structure should be positive for all cases. In the above equation it changes between positive and negative. This is because of the mode shape having the same initial slope, but the deflection of the top is alternating between positive and negative. So in this case I will take the absolute of the equations, thus

$$h_e = \frac{2.H}{\pi.n} \qquad \text{for } n = 1, 3, 5\ldots$$

The Effective Mass is the proportion of the total mass that is excited by a deflected shape. This proportion can be calculated by using the following formula. This formula has been derived from modal analysis techniques and gives the Effective Mass for each a given mode shape.

$$m_e = \frac{\left[\int_0^H \varphi(x)\rho(x)r(x)dx\right]^2}{\int_0^H \varphi(x)\rho(x)\varphi(x)dx}$$

Note, for this example *r(x)* and $\rho(x)$ are both constant, and thus can be removed for the integral giving the following equation.

$$m_e = \rho(x)\frac{\left[\int_0^H \varphi(x)dx\right]^2}{\int_0^H [\varphi(x)]^2 dx}$$

$$m_e = \rho\frac{\left[\int_0^H \sin(\phi.x)dx\right]^2}{\int_0^H [\sin(\phi.x)]^2 dx}$$

$$m_e = \rho\frac{\left[\left[-\frac{1}{\phi}\cos(\phi.x)\right]_{x=0}^{H}\right]^2}{\frac{1}{2}\left[x-\frac{1}{\phi}\sin(\phi.x)\cos(\phi.x)\right]_{x=0}^{H}}$$

$$m_e = 2\rho\frac{\left[-\frac{1}{\phi}[\cos(\phi.H)-1]\right]^2}{H-\frac{1}{\phi}\sin(\phi.H)\cos(\phi.H)}$$

$$m_e = \frac{2\rho}{\phi^2}\frac{1}{H} \qquad \text{for } n = 1, 3, 5\ldots$$

$$m_e = \frac{8\rho.H^2}{\pi^2.n^2}\frac{1}{H} \qquad \text{for } n = 1, 3, 5\ldots$$

$$m_e = \frac{8}{\pi^2 . n^2} \rho . H$$ for n = 1, 3, 5…

Flexural Structure

Mode Shape and Frequency equations obtained from (Clough and Penzien 1993)

The governing equation of motion for a flexural structure is

$$EI\frac{\partial^4}{\partial x^4}u(x,t)=\rho\frac{\partial^2}{\partial t^2}u(x,t)$$

This is a fourth order Partial Differential Equation, the solution of which is not easily defined. The following is the analytical solution for the mode shapes, however in the thesis an analytical solution was used for computational ease.

Firstly, define the deflected shape as a function of two separate parameters, then rearrange to separate variables.

$$u(x,t)=Y(t)\varphi(x)$$

$$\frac{\varphi^{iv}(x)}{\varphi(x)}=\frac{\rho}{EI}\frac{Y''(t)}{Y(t)}=\phi^4=\frac{\rho}{EI}\omega^2$$

It should be noted that the first term gives the ϕ^4 and the second term gives ω^2.

A rearrangement of the equation gives

$$\omega^2=\frac{\phi^4 EI}{\rho}$$

And hence,

$$\omega=(\phi.H)^2\sqrt{\frac{EI}{\rho H^4}}$$

By setting

$$\frac{\varphi^{iv}(x)}{\varphi^{ii}(x)}=\phi^4$$

and obtaining a solution for the Mode shape gives

$$\varphi(x)=A_1\cos(\phi.x)+A_2\sin(\phi.x)+A_3\cosh(\phi.x)+A_4\sinh(\phi.x)$$

Applying the boundary conditions for a Cantilever beam

$$\varphi(0) = 0 \qquad \varphi'(0) = 0$$
$$M(H) = EI\varphi''(H) = 0 \qquad V(L) = EI\varphi'''(H) = 0$$

Gives

$$\varphi(x) = A_1\cos(0) + A_2\sin(0) + A_3\cosh(0) + A_4\sinh(0) = 0$$
$$\varphi'(x) = \phi(-A_1\sin(0) + A_2\cos(0) + A_3\sinh(0) + A_4\cosh(0)) = 0$$
$$\varphi''(x) = \phi^2(-A_1\cos(\phi.H) - A_2\sin(\phi.H) + A_3\cosh(\phi.H) + A_4\sinh(\phi.H)) = 0$$
$$\varphi'''(x) = \phi^3(A_1\cos(\phi.H) + A_2\sin(\phi.H) + A_3\cosh(\phi.H) + A_4\sinh(\phi.H)) = 0$$

Noting that $\cos(0) = \cosh(0) = 1$ and $\sin(0) = \sinh(0) = 0$ leads to

$$\varphi(x) = A_1 + A_3 = 0 \Rightarrow A_3 = -A_1$$
$$\varphi'(x) = A_2 + A_4 = 0 \Rightarrow A_4 = -A_2$$

$$\begin{bmatrix} (\cos(\phi.H) + \cosh(\phi.H)) & (\sin(\phi.H) + \sinh(\phi.H)) \\ (\sinh(\phi.H) - \sin(\phi.H)) & (\cos(\phi.H) + \cosh(\phi.H)) \end{bmatrix} \begin{Bmatrix} A_1 \\ A_2 \end{Bmatrix} = \begin{Bmatrix} 0 \\ 0 \end{Bmatrix}$$

For non-trivial solution, the determinate of the matrix must be equal to zero. Hence,

$$\sinh^2(\phi.H) - \sin^2(\phi.H) - \cos^2(\phi.H) - 2\cosh(\phi.H)\cos(\phi.H) - \cosh^2(\phi.H) = 0$$

Which can the further reduced to

$$\cos(\phi.H) = -\frac{1}{\cosh(\phi.H)}$$

Roots are found using the above equation. Note that as the value of ϕH increases, then the cosh(ϕH) term tends to infinity, thus ϕH can be found from just using the cos(ϕH) term.

$$(\phi.H)_1 = 1.875$$
$$(\phi.H)_2 = 4.694$$

$$(\phi.H)_3 = 7.855$$

Note, for higher modes

$$(\phi.H)_n \cong \frac{\pi.(2n-1)}{2} \qquad n = 4, 5, 6, 7\ldots$$

$$\omega_n = \frac{\pi^2.(2n-1)^2}{4}\sqrt{\frac{E.I}{\rho H^4}} \qquad n = 4, 5, 6, 7\ldots$$

$$T_n = \frac{1}{(2n-1)^2}\frac{8}{\pi}\sqrt{\frac{\rho.H^4}{E.I}} \qquad n = 4, 5, 6, 7\ldots$$

By using $T_n = \frac{k_n}{(2n-1)^2}\frac{8}{\pi}\sqrt{\frac{\rho.H^4}{E.I}}$, gives $k_n = \frac{\pi^2}{4}\frac{(2n-1)^2}{(\phi.H)^2}$; thus

$$k_1 = 0.702$$

$$k_2 = 1.008$$

$$k_3 = 1.000$$

$$k_n = 1 \qquad n = 4, 5, 6, 7\ldots$$

Using the first equation from the matrix, A_2 can be expressed in terms of A_1.

$$A_2 = -\frac{(\cos(\phi.H)+\cosh(\phi.H))}{(\sin(\phi.H)+\sinh(\phi.H))}A_1$$

Thus along with $A_3 = -A_1$ and $A_4 = -A_2$ gives

$$\varphi(x) = A_1[\cos(\phi.x)-\cosh(\phi.x)-\lambda(\sin(\phi.x)-\sinh(\phi.x))]$$

Where $\lambda = \frac{\cos(\phi.H)+\cosh(\phi.H)}{\sin(\phi.H)+\sinh(\phi.H)}$ and the amplitude coefficient A_1 is assumed to be 1.

$$h_e = \frac{\int_0^H \varphi(x).x.dx}{\int_0^H \varphi(x).dx}$$

$$h_e = \frac{\int_0^H \left[x.\cos(\phi.x) - x.\cosh(\phi.x) - \lambda.x.\sin(\phi.x) + \lambda.x.\sinh(\phi.x)\right]dx}{\int_0^H \left[\cos(\phi.x) - \cosh(\phi.x) - \lambda.\sin(\phi.x) + \lambda.\sinh(\phi.x)\right].dx}$$

$$h_e = \frac{\frac{1}{\phi}\left[\left(\frac{\cos(\phi.x)}{\phi^2} - \frac{x.\sin(\phi.x)}{\phi}\right) - \left(-\frac{\cosh(\phi.x)}{\phi^2} + \frac{x.\sinh(\phi.x)}{\phi}\right) - \lambda\left(\frac{\sin(\phi.x)}{\phi^2} - \frac{x.\cos(\phi.x)}{\phi}\right) + \lambda\left(-\frac{\sinh(\phi.x)}{\phi^2} + \frac{x.\cosh(\phi.x)}{\phi}\right)\right]_{x=0}^{H}}{\frac{1}{\phi}\left[\sin(\phi.x) - \sinh(\phi.x) + \lambda.\cos(\phi.x) - \lambda.\cosh(\phi.x)\right]_{x=0}^{H}}$$

$$h_e = \frac{\frac{1}{\phi}\left[\left(\frac{\cos(\phi.H)}{\phi^2} - \frac{H.\sin(\phi.H)}{\phi}\right) - \left(-\frac{\cosh(\phi.H)}{\phi^2} + \frac{H.\sinh(\phi.H)}{\phi}\right) - \lambda\left(\frac{\sin(\phi.H)}{\phi^2} - \frac{H.\cos(\phi.H)}{\phi}\right) + \lambda\left(-\frac{\sinh(\phi.H)}{\phi^2} + \frac{H.\cosh(\phi.H)}{\phi}\right)\right]}{\frac{1}{\phi}\left[\sin(\phi.H) - \sinh(\phi.H) + \lambda.\cos(\phi.H) - \lambda.\cosh(\phi.H)\right] - \frac{1}{\phi}\left[0 - 0 + \lambda - \lambda\right]}$$

$$- \frac{\frac{1}{\phi}\left[\frac{1}{\phi^2} + \frac{1}{\phi^2}\right]}{\frac{1}{\phi}\left[\sin(\phi.H) - \sinh(\phi.H) + \lambda.\cos(\phi.H) - \lambda.\cosh(\phi.H)\right] - \frac{1}{\phi}\left[0 - 0 + \lambda - \lambda\right]}$$

$$h_e = \frac{\frac{1}{\phi^2}\left[\left(\cos(\phi.H) - \phi.H.\sin(\phi.H)\right) - \left(-\cosh(\phi.H) + \phi.H.\sinh(\phi.H)\right) - \lambda\left(\sin(\phi.H) - \phi.H.\cos(\phi.H)\right) + \lambda\left(-\sinh(\phi.H) + \phi.H.\cosh(\phi.H)\right)\right] - \frac{2}{\phi^2}}{\left[\sin(\phi.H) - \sinh(\phi.H) + \lambda.\cos(\phi.H) - \lambda.\cosh(\phi.H)\right]}$$

$$m_e = \frac{\left[\int_0^H \varphi(x)\rho(x)r(x)dx\right]^2}{\int_0^H \varphi(x)\rho(x)\varphi(x)dx}$$

$$m_e = \rho\frac{\left[\int_0^H \left[\cos(\phi.x) - \cosh(\phi.x) - \lambda.\sin(\phi.x) + \lambda.\sinh(\phi.x)\right].dx\right]^2}{\int_0^H \left[\varphi(x)\right]^2 dx}$$

$$m_e = \rho\frac{\left[\frac{1}{\phi}\left[\sin(\phi.x) - \sinh(\phi.x) + \lambda.\cos(\phi.x) - \lambda.\cosh(\phi.x)\right]_{x=0}^{H}\right]^2}{\int_0^H \left[\varphi(x)\right]^2 dx}$$

$$m_e = \rho\frac{\frac{1}{\phi^2}\left[\sin(\phi.H) - \sinh(\phi.H) + \lambda.\cos(\phi.H) - \lambda.\cosh(\phi.H)\right]^2}{\int_0^H \left[\varphi(x)\right]^2 dx}$$

$$\left[\varphi(x)\right]^2 = \cos^2(\phi.x) + \cosh^2(a.x) + \lambda^2\sin^2(a.x) + \lambda^2\sinh^2(a.x) - 2\cos(a.x)\cosh(a.x) - 2\lambda\sin(a.x)\cos(a.x)$$
$$+ 2\lambda\cos(a.x)\sinh(a.x) + 2\lambda\sin(a.x)\cosh(a.x) - 2\lambda\sinh(a.x)\cosh(a.x) - 2\lambda^2\sin(a.x)\sinh(a.x)$$

$$\int_0^H \left[\varphi(x)\right]^2 dx = \int_0^H \left[\cos^2(\phi.x) + \cosh^2(\phi.x) + \lambda^2\sin^2(\phi.x) + \lambda^2\sinh^2(\phi.x) - 2\cos(\phi.x)\cosh(\phi.x) - 2\lambda\sin(\phi.x)\cos(\phi.x)\right.$$
$$\left. + 2\lambda\cos(\phi.x)\sinh(\phi.x) + 2\lambda\sin(\phi.x)\cosh(\phi.x) - 2\lambda\sinh(\phi.x)\cosh(\phi.x) - 2\lambda^2\sin(\phi.x)\sinh(\phi.x)\right]dx$$

$$\int_0^H [\varphi(x)]^2\,dx = \left[\frac{1}{2}(x+\frac{1}{\phi}\sin(\phi.x)\cos(\phi.x)) + \frac{\lambda^2}{2}(x-\frac{1}{\phi}\sin(\phi.x)\cos(\phi.x)) + (\frac{1}{4\phi}\sinh(\phi.x)+\frac{x}{2}) + \lambda^2(\frac{1}{4\phi}\sinh(\phi.x)-\frac{x}{2})\right.$$
$$-\frac{1}{\phi}(\sinh(\phi.x)\cos(\phi.x)+\cosh(\phi.x)\sin(\phi.x)) + \frac{\lambda}{2\phi}\cos(2\phi.x) - \frac{\lambda}{\phi}(\cosh(\phi.x)\cos(\phi.x)+\sinh(\phi.x)\sin(\phi.x))$$
$$\left.+\frac{\lambda}{\phi}(\sinh(\phi.x).\sin(\phi.x)-\cosh(\phi.x)\cos(\phi.x)) + \frac{\lambda}{2\phi}\cosh(2\phi.x) - \frac{\lambda^2}{\phi}(\cosh(\phi.x)\sin(\phi.x)-\sinh(\phi.x)\cos(\phi.x))\right]_{x=0}^{H}$$

$$\int_0^H [\varphi(x)]^2\,dx = \frac{1}{\phi}\left[\frac{1}{2}(\phi.x+\sin(\phi.x)\cos(\phi.x)) + \frac{\lambda^2}{2}(\phi.x-\sin(\phi.x)\cos(\phi.x)) + (\frac{1}{4}\sinh(\phi.x)+\frac{\phi.x}{2}) + \lambda^2(\frac{1}{4}\sinh(\phi.x)-\frac{\phi.x}{2})\right.$$
$$-(\sinh(\phi.x)\cos(\phi.x)+\cosh(\phi.x)\sin(\phi.x)) + \frac{\lambda}{2}\cos(2\phi.x) - \lambda(\cosh(\phi.x)\cos(\phi.x)+\sinh(\phi.x)\sin(\phi.x))$$
$$\left.+\lambda(\sinh(\phi.x).\sin(\phi.x)-\cosh(\phi.x)\cos(\phi.x)) + \frac{\lambda}{2}\cosh(2\phi.x) - \lambda^2(\cosh(\phi.x)\sin(\phi.x)-\sinh(\phi.x)\cos(\phi.x))\right]_{x=0}^{H}$$

$$\int_0^H [\varphi(x)]^2\,dx = \frac{1}{\phi}\left[\frac{1}{2}(\phi.H+\sin(\phi.H)\cos(\phi.H)) + \frac{\lambda^2}{2}(\phi.H-\sin(\phi.H)\cos(\phi.H)) + (\frac{1}{4}\sinh(\phi.H)+\frac{\phi.H}{2}) + \lambda^2(\frac{1}{4}\sinh(\phi.H)-\frac{\phi.H}{2})\right.$$
$$-(\sinh(\phi.H)\cos(\phi.H)+\cosh(\phi.H)\sin(\phi.H)) + \frac{\lambda}{2}\cos(2\phi.H) - \lambda(\cosh(\phi.H)\cos(\phi.H)+\sinh(\phi.H)\sin(\phi.H))$$
$$\left.+\lambda(\sinh(\phi.H).\sin(\phi.H)-\cosh(\phi.H)\cos(\phi.H)) + \frac{\lambda}{2}\cosh(2\phi.H) - \lambda^2(\cosh(\phi.H)\sin(\phi.H)-\sinh(\phi.H)\cos(\phi.H))\right]$$
$$-\frac{1}{\phi}\left[\frac{1}{2}(0+\sin(0)\cos(0)) + \frac{\lambda^2}{2}(0-\sin(0)\cos(0)) + (\frac{1}{4}\sinh(0)+\frac{0}{2}) + \lambda^2(\frac{1}{4}\sinh(0)-\frac{0}{2})\right.$$
$$-(\sinh(0)\cos(0)+\cosh(0)\sin(0)) + \frac{\lambda}{2}\cos(0) - \lambda(\cosh(0)\cos(0)+\sinh(0)\sin(0))$$
$$\left.+\lambda(\sinh(0).\sin(0)-\cosh(0)\cos(0)) + \frac{\lambda}{2}\cosh(0) - \lambda^2(\cosh(0)\sin(0)-\sinh(0)\cos(0))\right]$$

$$\int_0^H [\varphi(x)]^2\,dx = \frac{1}{\phi}\Bigg[\frac{1}{2}(\phi.H+\sin(\phi.H)\cos(\phi.H))+\frac{\lambda^2}{2}(\phi.H-\sin(\phi.H)\cos(\phi.H))+(\frac{1}{4}\sinh(\phi.H)+\frac{\phi.H}{2})+\lambda^2(\frac{1}{4}\sinh(\phi.H)-\frac{\phi.H}{2})$$
$$-(\sinh(\phi.H)\cos(\phi.H)+\cosh(\phi.H)\sin(\phi.H))+\frac{\lambda}{2}\cos(2\phi.H)-\lambda(\cosh(\phi.H)\cos(\phi.H)+\sinh(\phi.H)\sin(\phi.H))$$
$$+\lambda(\sinh(\phi.H).\sin(\phi.H)-\cosh(\phi.H)\cos(\phi.H))+\frac{\lambda}{2}\cosh(2\phi.H)-\lambda^2(\cosh(\phi.H)\sin(\phi.H)-\sinh(\phi.H)\cos(\phi.H))\Bigg]+\frac{\lambda}{\phi}$$

Combined Shear and Flexural Structure

Mode Shape and Frequency equations obtained from (Clough and Penzien 1993)

The governing equation of motion for the structure is

$$EI\frac{\partial^4}{\partial x^4}u(x,t)+GA_s\frac{\partial^2}{\partial x^2}u(x,t)=\rho\frac{\partial^2}{\partial t^2}u(x,t)$$

$$u(x,t)=\varphi(x).Y(x)$$
$$\frac{\partial}{\partial t}u(x,t)=\varphi(x).Y^{i}(x)$$
$$\frac{\partial^2}{\partial t^2}u(x,t)=\varphi(x).Y^{ii}(x)$$

$$\frac{\partial}{\partial x}u(x,t)=\varphi^{i}(x).Y(x)$$
$$\frac{\partial^2}{\partial x^2}u(x,t)=\varphi^{ii}(x).Y(x)$$
$$\frac{\partial^3}{\partial x^3}u(x,t)=\varphi^{iii}(x).Y(x)$$
$$\frac{\partial^4}{\partial x^4}u(x,t)=\varphi^{iv}(x).Y(x)$$

$$EI\varphi^{iv}(x).Y(t)+GA_s\varphi^{ii}(x).Y(t)=\rho\varphi(x).Y^{ii}(t)$$

$$\frac{\varphi^{iv}(x)}{\varphi(x)}+\frac{GA_s}{EI}\frac{\varphi^{ii}(x)}{\varphi(x)}=\frac{\rho}{EI}\frac{Y^{ii}(t)}{Y(t)}\equiv\phi^4-\frac{GA_s}{EI}\phi^2=\frac{\rho}{EI}\omega^2$$

$$\varphi(x)=C\exp(sx)$$
$$\frac{\partial}{\partial x}\varphi(x)=Cs\exp(sx)$$
$$\frac{\partial^2}{\partial x^2}\varphi(x)=Cs^2\exp(sx)$$
$$\frac{\partial^3}{\partial x^3}\varphi(x)=Cs^3\exp(sx)$$
$$\frac{\partial^4}{\partial x^4}\varphi(x)=Cs^4\exp(sx)$$

$$\frac{Cs^4\exp(sx)}{C\exp(sx)}+\frac{GA_s}{EI}\frac{Cs^2\exp(sx)}{C\exp(sx)}=\phi^4-\frac{GA_s}{EI}\phi^2$$

$$\left[s^4+\frac{GA_s}{EI}s^2\right]C\exp(sx)=\left[\phi^4-\frac{GA_s}{EI}\phi^2\right]C\exp(sx)$$

$$\left[s^4-\phi^4+\frac{GA_s}{EI}\left(s^2+\phi^2\right)\right]C\exp(sx)=0$$

Gives

$$s^4-\phi^4+\frac{GA_s}{EI}\left(s^2+\phi^2\right)=0$$

Note that this can be arranged to give

$$s^4+\frac{GA_s}{EI}s^2-\left(\phi^4+\frac{GA_s}{EI}\phi^2\right)=0$$

Which is a quadratic

$$a=1$$

$$b=\frac{GA_s}{EI}$$

$$c=\left(\frac{GA_s}{EI}\phi^2-\phi^4\right)$$

$$s^2=\frac{-b\pm\sqrt{b^2-4ac}}{2a}$$

$$s^2=\frac{-\frac{GA_s}{EI}\pm\sqrt{\left(\frac{GA_s}{EI}\right)^2+4(1)\left(\frac{GA_s}{EI}\phi^2-\phi^4\right)}}{2(1)}$$

$$s^2=-\frac{GA_s}{2EI}\pm\sqrt{\left(\frac{GA_s}{2EI}\right)^2+\phi^4-\frac{GA_s}{EI}\phi^2}$$

$$\phi^4-\frac{GA_s}{EI}\phi^2+\left(\frac{GA_s}{EI}\right)^2=\left(\phi^2-\frac{GA_s}{2EI}\right)^2$$

thus

$$s^2=-\frac{GA_s}{2EI}\pm\left(\phi^2-\frac{GA_s}{2EI}\right)$$

$$s^2 = -\phi^2,\ \phi^2 - \frac{GA_s}{EI}$$

$$s = i\phi, -i\phi,\ \sqrt{\phi^2 - \frac{GA_s}{EI}},\ -\sqrt{\phi^2 - \frac{GA_s}{EI}}$$

hence

$$\varphi(x) = C_1 \exp(i\phi x) + C_2 \exp(-i\phi x) + C_3 \exp\left(\sqrt{\phi^2 - \frac{GA_s}{EI}}x\right) + C_4 \exp\left(-\sqrt{\phi^2 - \frac{GA_s}{EI}}x\right)$$

or alternatively

$$\varphi(x) = B_1 \sin(\phi x) + B_2 \cos(\phi x) + B_3 \sinh\left(\sqrt{\phi^2 - \frac{GA_s}{EI}}x\right) + B_4 \cosh\left(\sqrt{\phi^2 - \frac{GA_s}{EI}}x\right)$$

$$\left[\frac{EI}{GA_s}\left(s^4-\phi^4\right)+s^2-\phi^2\right]C\exp(sx)=0$$

Gives

$$\frac{EI}{GA_s}\left(s^4-\phi^4\right)+s^2-\phi^2=0$$

Note that this can be arranged to give

$$\frac{EI}{GA_s}s^4+s^2-\left(\frac{EI}{GA_s}\phi^4+\phi^2\right)=0$$

Which is a quadratic

$$a = \frac{EI}{GA_s}$$

$$b = 1$$

$$c = -\left(\frac{EI}{GA_s}\phi^4 + \phi^2 \right)$$

$$s^2 = \frac{-b \pm \sqrt{b^2 - 4ac}}{2a}$$

$$s^2 = \frac{-1 \pm \sqrt{1^2 + 4\left(\frac{EI}{GA_s} \right)\left(\frac{EI}{GA_s}\phi^4 + \phi^2 \right)}}{2\left(\frac{EI}{GA_s} \right)}$$

$$s^2 = \frac{-\frac{GA_s}{EI} \pm \sqrt{1 + 4\left(\frac{EI}{GA_s} \right)^2 \phi^4 + 4\frac{EI}{GA_s}\phi^2}}{2\left(\frac{EI}{GA_s} \right)}$$

$$4\left(\frac{EI}{GA_s} \right)^2 \phi^4 + 4\frac{EI}{GA_s}\phi^2 + 1 = \left(2\frac{EI}{GA_s}\phi^2 + 1 \right)^2$$

thus

$$s^2 = \frac{-1 \pm \left(2\frac{EI}{GA_s}\phi^2 + 1 \right)}{2\left(\frac{EI}{GA_s} \right)}$$

$$s^2 = \frac{\left(\frac{EI}{GA_s} \right)\phi^2}{\left(\frac{EI}{GA_s} \right)}, \quad i^2 \frac{\left(\frac{EI}{GA_s}\phi^2 + 1 \right)}{\left(\frac{EI}{GA_s} \right)}$$

Appendix B: Non-Linear Factor

Skinner et al. Derivation

This Non-Linear factor is for a Bi-Linear Isolator and is essentially producing the ratio of the Hysteretic Loop to the area enclosed by a rectangle that reaches the minimum and maximum points achieved for a symmetric displacement and thus it is similar to the hysteretic damping factor ζ_h. The equation for this is

$$NL = Q_y / S_b - X_y / X_b$$

where Q_y is the yield strength, S_b is the maximum force obtained, X_y is the yield displacement and X_b is the displacement at maximum force. This means that the most of the Isolator parameters are required for the calculation of the non-linearity factor and this it becomes an iterative procedure. For this Thesis the above equation shall be reworked as follows.

Define

$$\mu = \frac{X_b}{X_y} \text{ and } r = \frac{k_2}{k_1}$$

The equation for the period of an object based on its mass and stiffness is

$$T = 2\pi\sqrt{\frac{m}{k}} \text{ or } k = m\left(\frac{2\pi}{T}\right)^2, \text{ thus } r = \left(\frac{T_1}{T_2}\right)^2$$

From the Bi-Linear line of the Backbone curve for the Isolator we obtain

$$k_1 = \frac{Q_y}{X_y} \text{ and } k_2 = \frac{S_b - Q_y}{X_b - X_y}$$

So

$$r = \frac{k_2}{k_1} = \frac{S_b - Q_y}{X_b - X_y} \cdot \frac{X_y}{Q_y}$$

$$r = \frac{S_b - Q_y}{Q_y} \cdot \frac{X_y}{X_b - X_y}$$

$$r = \frac{S_b/Q_y - 1}{1} \cdot \frac{1}{X_b/X_y - 1}$$

$$r = \frac{S_b/Q_y - 1}{\mu - 1}$$

$$\frac{S_b}{Q_y} = 1 + r(\mu - 1)$$

Recall

$$NL = \frac{Q_y}{S_b} - \frac{X_y}{X_b}$$

$$NL = \frac{1}{1 + r(\mu - 1)} - \frac{1}{\mu}$$

$$NL = \frac{\mu - (1 + r(\mu - 1))}{\mu(1 + r(\mu - 1))}$$

$$NL = \frac{(\mu - 1) - r(\mu - 1)}{\mu(1 + r(\mu - 1))}$$

$$NL = \frac{(\mu - 1)(1 - r)}{\mu(1 + r(\mu - 1))}$$

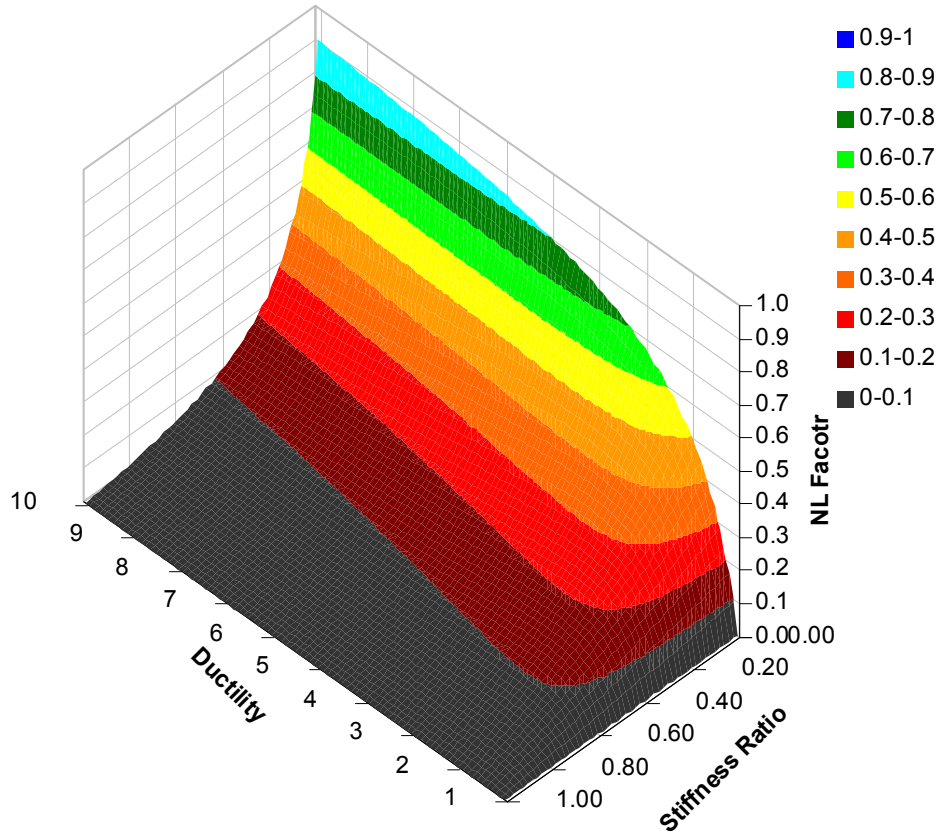

Figure B.0.1 3D plot of Non-Linear factor against the parameters ductility, μ, and Stiffness Ratio, r.

Appendix C: Elevation of Building

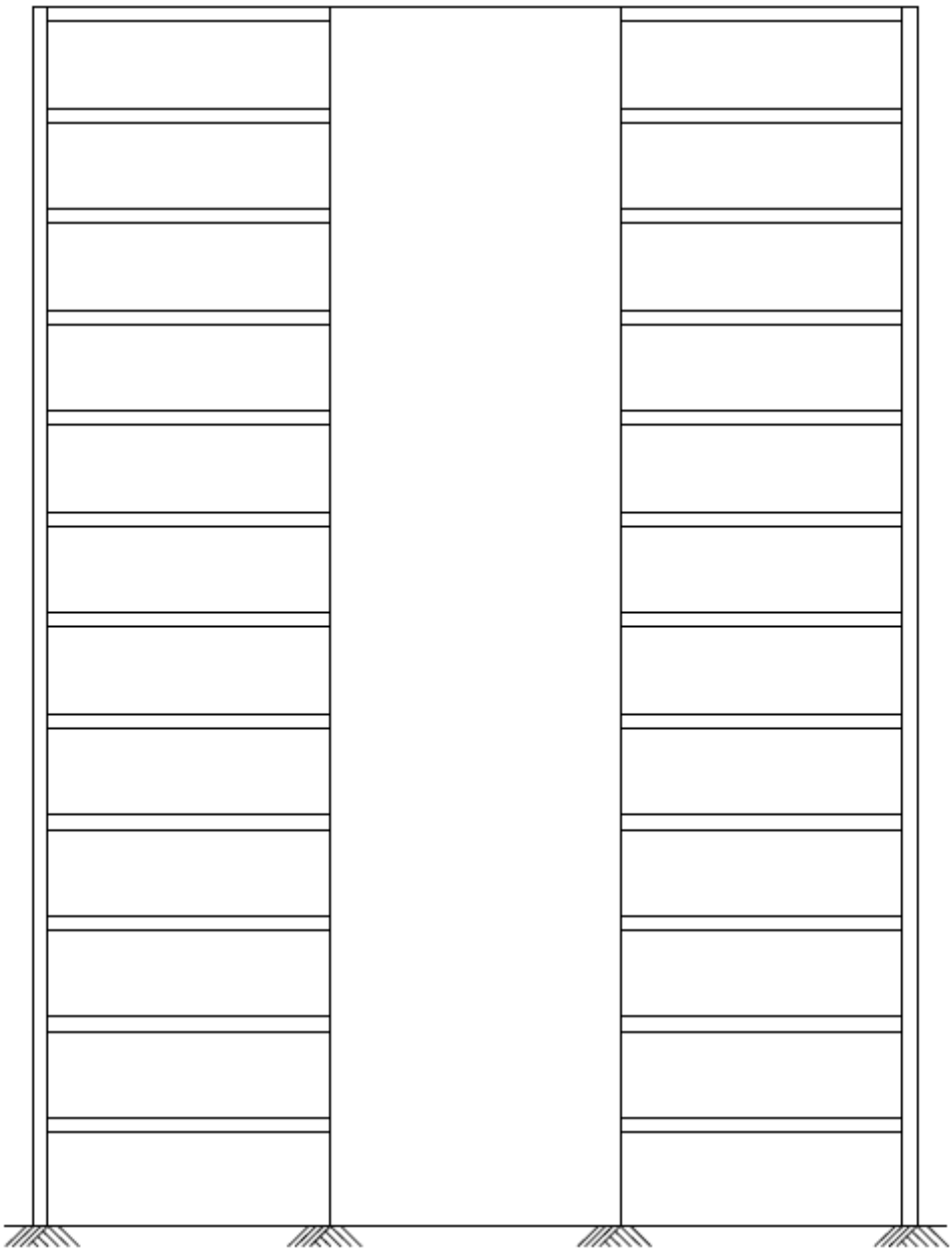

Figure C.0.1 Elevation of structure used in analysis

The building is a total of 28m high; each floor height is 3.5m. The width of the structure is 30m with two 10m bays and a 10m wall in the centre.

Appendix D: Moment-Axial Force Interaction Diagrams

The following plots are the moment-axial force interaction diagrams for the columns and shear walls used in this thesis. They have been plotted using a spreadsheet created for the purpose of calculating strains, and hence stresses, forces and moments, for a given neutral axis depth and the strain of the concrete on the compression edge of the element being checked. For both columns and wall have symmetric detailing and reinforcement layout, hence the graphs are for both positive and negative moments.

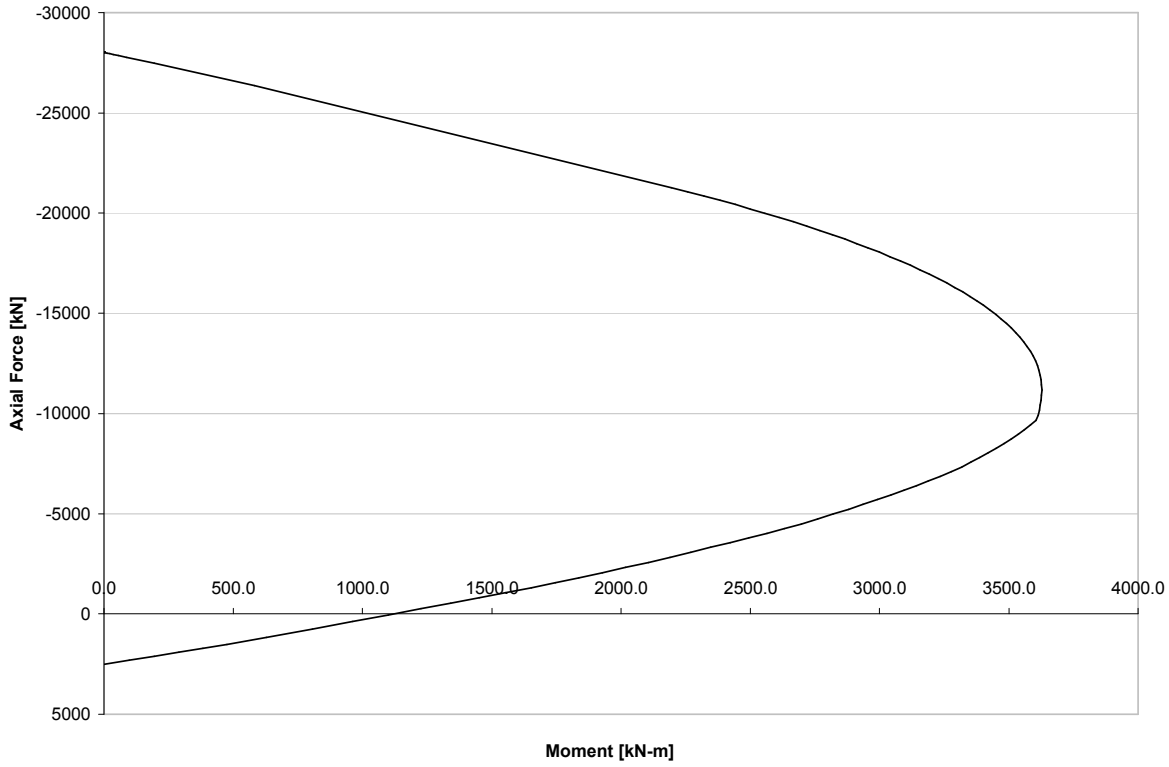

Figure D.0.1 Plot of column M-N interaction

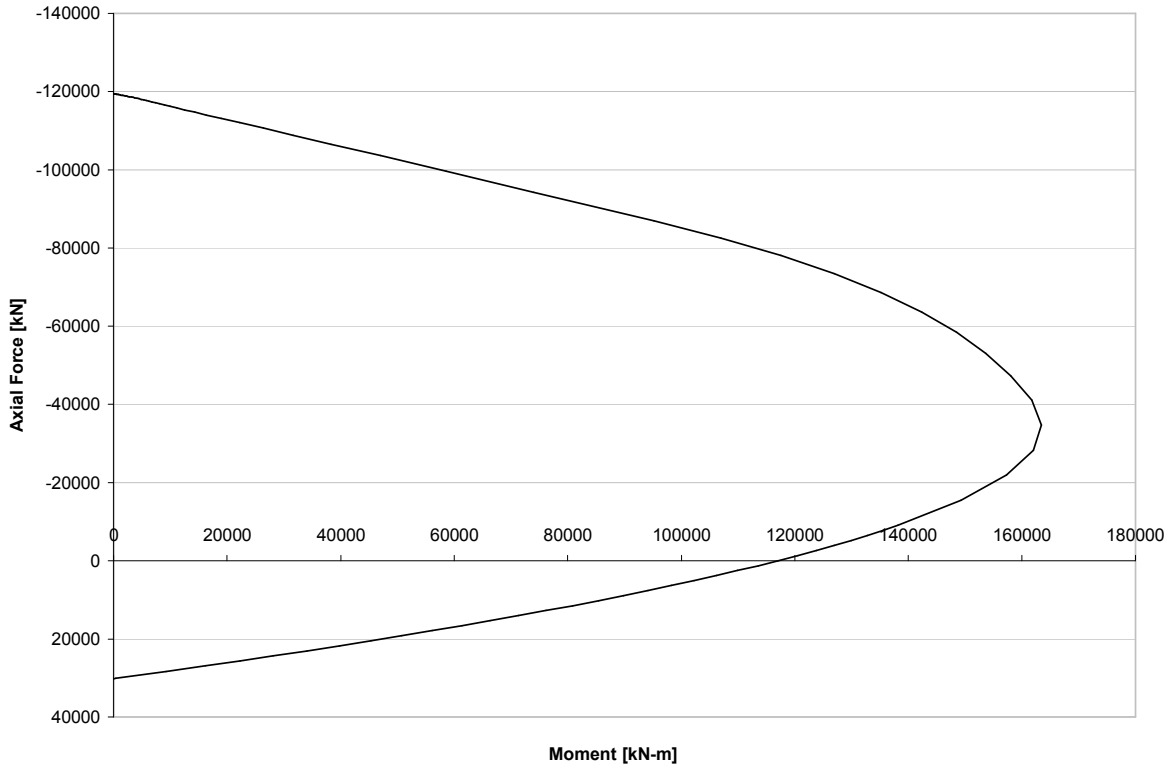

Figure D.0.2 Plot of wall M-N interaction

Appendix E: Ruaumoko Input Data

The following is the data from an input file for an isolated structure with no mass shift. The isolator parameters are yield strength equal to 5% of the structural weight, an initial period of 1.5 seconds and a post yield period of 4.0 seconds.

```
   Structure: Shear Wall 8-Storey Office
*
*   EIGHT STOREY OFFICE BLOCK, BASED ON THE NZS 1170 CODE
*       NZS 1170.0   General Principles
*       NZS 1170.1   Permanent, Imposed and Other Actions
*       NZS 1170.2   Wind Actions
*       NZS 1170.5   Earthquake Actions: New Zealand
*
*   This Structure was Designed as part of a Master Thesis conducted at the University
*       of Canterbury, New Zealand.
*
*   This Data file uses the following Units
*   Length  ==  Metres       [m]
*   Time    ==  Seconds      [s]
*   Mass    ==  kiloNewtons  [kN]
*
*   Alastair Waller
*

!  IPANAL  IFMT    IPLAS   IPCONM  ICTYPE  IPVERT  INLGEO  IPNF    IZERO   ORTHO   IMODE
   2       1       1       0       0       0       0       0       1       0       0
!  NNP     NMEM    NTYPE   M       MODE1   MODE2   GRAV    C1      C2      DT      TIME    FACTOR
   94      43      8       6       1       4       9.81    5       5       0.01    150     1.0
!  KP      KPA     KPLOT   JOUT    DSTORT  DFACT   XMAX    YMAX    NLEVEL  NUP     IRESID  KDUMP
   0       5       5       0       1.0     1.0     5       5       9       2       0       0
!  MAXIT   MAXCIT  FTEST   WAVEX   WAVEY   THETA   DXMAX   DYMAX   D       OMEGA   F
   5       5       0.0001  0       0       0       5       5       0       0       0.1


NODES
! NODE X   Y       RX      RY      RZ      KUP1    KUP2    KUP3    IOUT
! MAIN NODES
  1       0.0     0.0     0       1       1       0       0       0       1
  2       0.0     3.5     0       0       0       0       0       0       1
  3       0.0     7.0     0       0       0       0       0       0       1
  4       0.0     10.5    0       0       0       0       0       0       1
  5       0.0     14.0    0       0       0       0       0       0       1
  6       0.0     17.5    0       0       0       0       0       0       1
  7       0.0     21.0    0       0       0       0       0       0       1
  8       0.0     24.5    0       0       0       0       0       0       1
  9       0.0     28.0    0       0       0       0       0       0       1
 10       15.0    0.0     0       1       1       1       0       0       1
 11       15.0    3.5     0       0       0       2       0       0       1
 12       15.0    7.0     0       0       0       3       0       0       1
 13       15.0    10.5    0       0       0       4       0       0       1
```

```
 14       15.0    14.0    0       0       0       5       0       0       1
 15       15.0    17.5    0       0       0       6       0       0       1
 16       15.0    21.0    0       0       0       7       0       0       1
 17       15.0    24.5    0       0       0       8       0       0       1
 18       15.0    28.0    0       0       0       9       0       0       1
 19       30.0    0.0     0       1       1       1       0       0       1
 20       30.0    3.5     0       0       0       2       0       0       1
 21       30.0    7.0     0       0       0       3       0       0       1
 22       30.0    10.5    0       0       0       4       0       0       1
 23       30.0    14.0    0       0       0       5       0       0       1
 24       30.0    17.5    0       0       0       6       0       0       1
 25       30.0    21.0    0       0       0       7       0       0       1
 26       30.0    24.5    0       0       0       8       0       0       1
 27       30.0    28.0    0       0       0       9       0       0       1
! INTERMEDIATE NODES
! LEFT COLUMN
 28       0.0     3.1     0       0       0       0       0       0       1
 29       0.0     3.9     0       0       0       0       0       0       1
 30       0.0     6.6     0       0       0       0       0       0       1
 31       0.0     7.4     0       0       0       0       0       0       1
 32       0.0     10.1    0       0       0       0       0       0       1
 33       0.0     10.9    0       0       0       0       0       0       1
 34       0.0     13.6    0       0       0       0       0       0       1
 35       0.0     14.4    0       0       0       0       0       0       1
 36       0.0     17.1    0       0       0       0       0       0       1
 37       0.0     17.9    0       0       0       0       0       0       1
 38       0.0     20.6    0       0       0       0       0       0       1
 39       0.0     21.4    0       0       0       0       0       0       1
 40       0.0     24.1    0       0       0       0       0       0       1
 41       0.0     24.9    0       0       0       0       0       0       1
 42       0.0     27.6    0       0       0       0       0       0       1
! RIGHT COLUMN
 43       30.0    3.1     0       0       0       0       0       0       1
 44       30.0    3.9     0       0       0       0       0       0       1
 45       30.0    6.6     0       0       0       0       0       0       1
 46       30.0    7.4     0       0       0       0       0       0       1
 47       30.0    10.1    0       0       0       0       0       0       1
 48       30.0    10.9    0       0       0       0       0       0       1
 49       30.0    13.6    0       0       0       0       0       0       1
 50       30.0    14.4    0       0       0       0       0       0       1
 51       30.0    17.1    0       0       0       0       0       0       1
 52       30.0    17.9    0       0       0       0       0       0       1
 53       30.0    20.6    0       0       0       0       0       0       1
 54       30.0    21.4    0       0       0       0       0       0       1
 55       30.0    24.1    0       0       0       0       0       0       1
 56       30.0    24.9    0       0       0       0       0       0       1
 57       30.0    27.6    0       0       0       0       0       0       1
! LEFT COLUMN; BEAMS NODES
 58       0.5     3.5     0       0       0       0       0       0       1
 59       0.5     7.0     0       0       0       0       0       0       1
 60       0.5     10.5    0       0       0       0       0       0       1
 61       0.5     14.0    0       0       0       0       0       0       1
 62       0.5     17.5    0       0       0       0       0       0       1
```

```
 63       0.5    21.0   0      0      0      0      0      0      1
 64       0.5    24.5   0      0      0      0      0      0      1
 65       0.5    28.0   0      0      0      0      0      0      1
! LEFT WALL SIDE; BEAMS NODES
 66       9.5    3.5    0      0      0      0      0      0      1
 67       9.5    7.0    0      0      0      0      0      0      1
 68       9.5    10.5   0      0      0      0      0      0      1
 69       9.5    14.0   0      0      0      0      0      0      1
 70       9.5    17.5   0      0      0      0      0      0      1
 71       9.5    21.0   0      0      0      0      0      0      1
 72       9.5    24.5   0      0      0      0      0      0      1
 73       9.5    28.0   0      0      0      0      0      0      1
! RIGHT WALL SIDE; BEAMS NODES
 74       20.5   3.5    0      0      0      0      0      0      1
 75       20.5   7.0    0      0      0      0      0      0      1
 76       20.5   10.5   0      0      0      0      0      0      1
 77       20.5   14.0   0      0      0      0      0      0      1
 78       20.5   17.5   0      0      0      0      0      0      1
 79       20.5   21.0   0      0      0      0      0      0      1
 80       20.5   24.5   0      0      0      0      0      0      1
 81       20.5   28.0   0      0      0      0      0      0      1
! RIGHT COLUMN; BEAMS NODES
 82       29.5   3.5    0      0      0      0      0      0      1
 83       29.5   7.0    0      0      0      0      0      0      1
 84       29.5   10.5   0      0      0      0      0      0      1
 85       29.5   14.0   0      0      0      0      0      0      1
 86       29.5   17.5   0      0      0      0      0      0      1
 87       29.5   21.0   0      0      0      0      0      0      1
 88       29.5   24.5   0      0      0      0      0      0      1
 89       29.5   28.0   0      0      0      0      0      0      1
! BASE ISOLATION UNITS
 90       0.5    0.0    0      0      0      0      0      0      1
 91       9.5    0.0    0      0      0      0      0      0      1
 92       20.5   0.0    0      0      0      0      0      0      1
 93       29.5   0.0    0      0      0      0      0      0      1
! EXTRA NODE
 94       0.0    0.0    1      1      1      0      0      0      1

DRIFT ANGLE
 10  11  12  13  14  15  16  17  18

ELEMENTS
! N       MT     NODE1  NODE2  NODE3  NODE4  IOUT
! LEFT COLUMN
  1       1      1      2      1      28     1
  2       1      2      3      29     30     1
  3       1      3      4      31     32     1
  4       2      4      5      33     34     1
  5       2      5      6      35     36     1
  6       2      6      7      37     38     1
  7       3      7      8      39     40     1
  8       3      8      9      41     42     1
! SHEAR WALL
```

```
  9       4       10      11      10      11      1
 10       4       11      12      11      12      1
 11       4       12      13      12      13      1
 12       5       13      14      13      14      1
 13       5       14      15      14      15      1
 14       5       15      16      15      16      1
 15       6       16      17      16      17      1
 16       6       17      18      17      18      1
! RIGHT COLUMN
 17       1       19      20      19      43      1
 18       1       20      21      44      45      1
 19       1       21      22      46      47      1
 20       2       22      23      48      49      1
 21       2       23      24      50      51      1
 22       2       24      25      52      53      1
 23       3       25      26      54      55      1
 24       3       26      27      56      57      1
! LEFT BEAMS
 25       7       2       11      58      66      1
 26       7       3       12      59      67      1
 27       7       4       13      60      68      1
 28       7       5       14      61      69      1
 29       7       6       15      62      70      1
 30       7       7       16      63      71      1
 31       7       8       17      64      72      1
 32       7       9       18      65      73      1
! RIGHT BEAMS
 33       7       11      20      74      82      1
 34       7       12      21      75      83      1
 35       7       13      22      76      84      1
 36       7       14      23      77      85      1
 37       7       15      24      78      86      1
 38       7       16      25      79      87      1
 39       7       17      26      80      88      1
 40       7       18      27      81      89      1
! GROUND BEAMS
 41       7       1       10      90      91      1
 42       7       10      19      92      93      1
! BASE ISOLATION UNITS
 43       8       1       94      1       94      1

PROPS
! N       MTYPE   LABEL
! ITYPE   IPIN    ICOND   IHYST   ILOS    IDAMG   ICOL    IGA     IDUCT
! E       G       A       AS      I       WGT     END1    END2    FJ1     FJ2
! RA      RF      H1      H2      H3      H4      H5      H6      H7
! BETA0   BETAT   ALPHA
! M1      M2      V1      V2      AXIAL   AXPS    IOP
! PYT     PYC     MY1+    MY1-    MY2+    MY2-    MY3+    MY3-    MY4+    MY4-
! PYC     PB      MB      M1B     M2B     M0      PYT     IEND
! PYC     PB      MB      M0      PC      MC      PYT     IEND
! PYC     PB      MB      PC      MC      PYT     IEND
  1       FRAME   "BOTTOM COLUMN SECTION"
```

```
  1       0       0       2       0       0       0       0       0
 26.2e6   12.8e6  1       1       0.0236  0       0       0       0       0       ! Note: WGT =
24kN/m, included in Weight
  0.01    0.10    1.0     1.0
 2513.3   37834.8 3834.4  -3834.4 3834.4  -3834.4

  2       FRAME   "MIDDLE COLUMN SECTION"
  1       0       0       2       0       0       0       0       0
 26.2e6   12.8e6  1       1       0.0202  0       0       0       0       0       ! Note: WGT =
24kN/m, included in Weight
  0.01    0.08    1.0     1.0
 2513.3   37834.8 2994.5  -2994.5 2994.5  -2994.5

  3       FRAME   "TOP COLUMN SECTION"
  1       0       0       2       0       0       0       0       0
 26.2e6   12.8e6  1       1       0.0144  0       0       0       0       0       ! Note: WGT =
24kN/m, included in Weight
  0.01    0.05    1.0     1.0
 2513.3   37834.8 2017.9  -2017.9 2017.9  -2017.9

  4       FRAME   "BOTTOM WALL SECTION"
  1       0       0       2       0       0       0       0       0
 26.2e6   12.8e6  3.5     3.5     4.3707  0       0       0       0       0       ! Note: WGT =
60kN/m, included in Weight
  0.01    0.17    1.0     1.0
30188.7   152295.3 76992.4 -76992.4 76992.4 -76992.4

  5       FRAME   "MIDDLE WALL SECTION"
  1       0       0       2       0       0       0       0       0
 26.2e6   12.8e6  3.5     3.5     4.3707  0       0       0       0       0       ! Note: WGT =
60kN/m, included in Weight
  0.01    0.17    1.0     1.0
30188.7   152295.3 76992.4 -76992.4 76992.4 -76992.4

  6       FRAME   "TOP WALL SECTION"
  1       0       0       2       0       0       0       0       0
 26.2e6   12.8e6  3.5     3.5     4.3707  0       0       0       0       0       ! Note: WGT =
60kN/m, included in Weight
  0.01    0.17    1.0     1.0
30188.7   152295.3 76992.4 -76992.4 76992.4 -76992.4

  7       FRAME   "BEAM SECTION"
  1       0       0       2       0       0       0       0       0
 26.2e6   12.8e6  0.4     0.4     0.0031  0       0       0       0       0       ! Note: WGT =
9.6kN/m, included in Weight
  0.01    0.03    1.0     1.0
! PYT     PYC     MY1+    MY1-    MY2+    MY2-    MY3+    MY3-    MY4+    MY4-
 3317.5   17282.0 978     -978    978     -978

  8       SPRING "BASE ISOLATION"
! ITYPE   IHYST   ILOS    IDAMG   KX              KY      GJ      WGT     RF      RT      PSX
   PSY     PSZ     THETA   ITRUSS  IOP
```

```
     1    2      0      0      58340.0        0      0      0      0.14    0.14    0      0
   0      0      0             0
! FX+             FX-    FY+    FY-    MZ+    MZ-
  1631.0  1631.0 0.0    0.0    0.0    0.0
```

WEIGHTS

! N	WX	WY	WZ
1	930	0	0
2	930	0	0
3	930	0	0
4	930	0	0
5	930	0	0
6	930	0	0
7	930	0	0
8	930	0	0
9	713	0	0
10	1860	0	0
11	1860	0	0
12	1860	0	0
13	1860	0	0
14	1860	0	0
15	1860	0	0
16	1860	0	0
17	1860	0	0
18	1425	0	0
19	930	0	0
20	930	0	0
21	930	0	0
22	930	0	0
23	930	0	0
24	930	0	0
25	930	0	0
26	930	0	0
27	713	0	0
28	0	0	0
29	0	0	0
30	0	0	0
31	0	0	0
32	0	0	0
33	0	0	0
34	0	0	0
35	0	0	0
36	0	0	0
37	0	0	0
38	0	0	0
39	0	0	0
40	0	0	0
41	0	0	0
42	0	0	0
43	0	0	0
44	0	0	0
45	0	0	0

```
 46        0       0       0
 47        0       0       0
 48        0       0       0
 49        0       0       0
 50        0       0       0
 51        0       0       0
 52        0       0       0
 53        0       0       0
 54        0       0       0
 55        0       0       0
 56        0       0       0
 57        0       0       0
 58        0       0       0
 59        0       0       0
 60        0       0       0
 61        0       0       0
 62        0       0       0
 63        0       0       0
 64        0       0       0
 65        0       0       0
 66        0       0       0
 67        0       0       0
 68        0       0       0
 69        0       0       0
 70        0       0       0
 71        0       0       0
 72        0       0       0
 73        0       0       0
 74        0       0       0
 75        0       0       0
 76        0       0       0
 77        0       0       0
 78        0       0       0
 79        0       0       0
 80        0       0       0
 81        0       0       0
 82        0       0       0
 83        0       0       0
 84        0       0       0
 85        0       0       0
 86        0       0       0
 87        0       0       0
 88        0       0       0
 89        0       0       0

LOADS
! N       FX      FY      FM
  1       0       0       0
  2       0       0       0
  3       0       0       0
  4       0       0       0
  5       0       0       0
  6       0       0       0
```

7	0	0	0
8	0	0	0
9	0	0	0
10	0	0	0
11	0	0	0
12	0	0	0
13	0	0	0
14	0	0	0
15	0	0	0
16	0	0	0
17	0	0	0
18	0	0	0
19	0	0	0
20	0	0	0
21	0	0	0
22	0	0	0
23	0	0	0
24	0	0	0
25	0	0	0
26	0	0	0
27	0	0	0
28	0	0	0
29	0	0	0
30	0	0	0
31	0	0	0
32	0	0	0
33	0	0	0
34	0	0	0
35	0	0	0
36	0	0	0
37	0	0	0
38	0	0	0
39	0	0	0
40	0	0	0
41	0	0	0
42	0	0	0
43	0	0	0
44	0	0	0
45	0	0	0
46	0	0	0
47	0	0	0
48	0	0	0
49	0	0	0
50	0	0	0
51	0	0	0
52	0	0	0
53	0	0	0
54	0	0	0
55	0	0	0
56	0	0	0
57	0	0	0
58	0	0	0
59	0	0	0

```
60        0       0       0
61        0       0       0
62        0       0       0
63        0       0       0
64        0       0       0
65        0       0       0
66        0       0       0
67        0       0       0
68        0       0       0
69        0       0       0
70        0       0       0
71        0       0       0
72        0       0       0
73        0       0       0
74        0       0       0
75        0       0       0
76        0       0       0
77        0       0       0
78        0       0       0
79        0       0       0
80        0       0       0
81        0       0       0
82        0       0       0
83        0       0       0
84        0       0       0
85        0       0       0
86        0       0       0
87        0       0       0
88        0       0       0
89        0       0       0

EQUAKE
5       1       0.01    1    -1      0       0       1
```